Heterodimeric capping protein is required for stereocilia length and width regulation

Matthew R. Avenarius,[1]* Jocelyn F. Krey,[1]* Rachel A. Dumont,[1] Clive P. Morgan,[1] Connor B. Benson,[1] Sarath Vijayakumar,[2] Christopher L. Cunningham,[3] Deborah I. Scheffer,[4] David P. Corey,[4] Ulrich Müller,[3] Sherri M. Jones,[2] and Peter G. Barr-Gillespie[1]

[1]Oregon Hearing Research Center and Vollum Institute, Oregon Health and Science University, Portland, OR
[2]Department of Special Education and Communication Disorders, University of Nebraska-Lincoln, Lincoln, NE
[3]Department of Neuroscience, Johns Hopkins University, Baltimore, MD
[4]Department of Neurobiology, Harvard Medical School, Boston, MA

Control of the dimensions of actin-rich processes like filopodia, lamellipodia, microvilli, and stereocilia requires the coordinated activity of many proteins. Each of these actin structures relies on heterodimeric capping protein (CAPZ), which blocks actin polymerization at barbed ends. Because dimension control of the inner ear's stereocilia is particularly precise, we studied the CAPZB subunit in hair cells. CAPZB, present at ∼100 copies per stereocilium, concentrated at stereocilia tips as hair cell development progressed, similar to the CAPZB-interacting protein TWF2. We deleted *Capzb* specifically in hair cells using *Atoh1-Cre*, which eliminated auditory and vestibular function. *Capzb*-null stereocilia initially developed normally but later shortened and disappeared; surprisingly, stereocilia width decreased concomitantly with length. CAPZB2 expressed by in utero electroporation prevented normal elongation of vestibular stereocilia and irregularly widened them. Together, these results suggest that capping protein participates in stereocilia widening by preventing newly elongating actin filaments from depolymerizing.

Introduction

Actin-rich structures are widespread in biology, exploited by cells for force generation and rigidity in motility, adhesion, and other processes (Chhabra and Higgs, 2007; Michelot and Drubin, 2011). The vertebrate hair bundle, responsible for transduction of mechanical signals into receptor potentials in sensory hair cells, is a particularly striking example (Barr-Gillespie, 2015). Composed of actin-filled stereocilia arranged in a highly ordered fashion, the bundle is optimized for sensing auditory and vestibular stimuli. Stereocilia number (typically 30–300), height (1–50 µm), and diameter (0.1–0.5 µm) are all regulated precisely in auditory and vestibular organs. Formation of bundles takes place in multiple steps, described by Tilney's four stages (Tilney et al., 1992; Barr-Gillespie, 2015). In stage 1, hair cells complete their final mitoses, whereas in stage 2, stereocilia begin to sprout and form an initial staircase. Stereocilia stop growing during stage 3 and instead widen, develop their basal tapers, and form their rootlets; in stage 4, the stereocilia resume growing until they reach their final lengths. In chick, these steps are temporally segregated, but they may run together in mammals (Kaltenbach et al., 1994; Sekerková et al., 2011).

Like in many actin structures, barbed-end capping molecules control actin filament length in stereocilia. During the widening of Tilney's stage 3, stereocilia elongation at barbed ends ceases, which likely requires barbed-end actin cappers (Tilney and DeRosier, 1986). Likewise, maintenance of mature stereocilia length requires a balance of actin capping and severing (Narayanan et al., 2015). Several proteins with barbed-end capping activity have been identified in hair bundles. EPS8 and EPS8L2, which have capping activity in vitro (Hertzog et al., 2010), are found respectively on the tips of the longest and all other stereocilia (Furness et al., 2013). Gelsolin (GSN) is part of a stereocilia tip complex, and its loss leads to long and straggled stereocilia, especially in the cochlear apex (Mburu et al., 2010; Olt et al., 2014). Twinfilins TWF1 and TWF2 are both found in stereocilia (Peng et al., 2009; Rzadzinska et al., 2009; Shin et al., 2013); although capping activity has been ascribed to the twinfilins, they also bind actin monomers, similar to GSN (Moseley et al., 2006). Finally, heterodimeric capping protein (CAPZ) binds to the barbed ends of actin filaments and prevents both polymerization and depolymerization (Caldwell et

*M.R. Avenarius and J.F. Krey contributed equally to this paper.

Correspondence to Peter G. Barr-Gillespie: gillespp@ohsu.edu

Abbreviations used: ABR, auditory brainstem response; DDA, data-dependent acquisition; DIA, data-independent acquisition; DPOAE, distortion-product otoacoustic emission; FWHM, full width at half-maximum; GSN, gelsolin; MS/MS, tandem mass spectrometry; P, postnatal day; PDH, pyruvate dehydrogenase; PSF, point spread function; riBAQ, relative intensity–based absolute quantification; VsEP, vestibular-evoked potential.

The Rockefeller University Press
J. Cell Biol. Vol. 216 No. 11 3861–3881
https://doi.org/10.1083/jcb.201704171

al., 1989). Capping protein was identified by mass spectrometry in chick utricle and cochlea bundles and was localized to stereocilia tips in cochlea (Shin et al., 2013; Avenarius et al., 2014). Although capping protein binds very tightly to actin barbed ends, its affinity can be reduced by specific regulators (Edwards et al., 2014).

During stage 3 in chick, stereocilia actin filaments increase in number from ∼100 to as many as 900 (Tilney and DeRosier, 1986). Although several mouse mutants have somewhat narrower stereocilia actin cores, the two genes most clearly associated with widening are *Grxcr1* and *Espn* (Odeh et al., 2010; Sekerková et al., 2011). Analysis of *Espn*^{jerker} heterozygotes, which do not have a behavioral phenotype, suggests that widening involves barbed-end growth of new actin filaments, initiating at the ankle region of the stereocilium (Sekerková et al., 2011). In *Espn*^{jerker} homozygotes, which have profoundly reduced auditory and vestibular function, stereocilia only partially lengthen and contain only 15–50% as many actin filaments as do controls; the stereocilia then shorten and disappear as development proceeds (Sekerková et al., 2011). Length therefore appears to be coordinated with width.

Here, we investigated the physiological role of capping protein in mouse hair bundles. We measured expression of capping protein subunits, as well as other actin cappers, using quantitative mass spectrometry. We also examined the physiological and morphological consequences of conditionally knocking out *Capzb* in hair cells, as well as effects on bundle structure caused by heterologous expression of MYC-CAPZB. Together, our experiments suggest that heterodimeric capping protein plays an integral role in the coordination of stereocilia length and width.

Results

Mass spectrometry identification of actin cappers

To identify and quantify actin-capper molecules in purified hair bundles from utricles, we examined chick and mouse mass-spectrometry datasets containing bundles and epithelium (Shin et al., 2013; Krey et al., 2015; Wilmarth et al., 2015); data are in Table S1. The most abundant cappers found in chick utricle bundles were (in order) CAPZB, TWF2, CAPZA1, CAPZA2, EPS8L2, GSN, TWF1, and EPS8 (Fig. 1 A); we only found evidence for the CAPZB2 splice form of CAPZB. We estimated that ∼600 heterodimeric capping proteins, which consist of one CAPZA subunit and one CAPZB2 subunit, were present in the average chick stereocilium of 400,000 actin molecules (Fig. 1 C), greater than the ∼200 filaments per stereocilium (Shin et al., 2013). In mouse utricle bundles, we found (in order) GSN, TWF2, CAPZA1, CAPZA2, CAPZB, TWF1, EPS8L2, and EPS8 (Fig. 1 B). GSN was present at ∼1,500 molecules per stereocilium, whereas capping protein heterodimers were present at only ∼100 molecules per stereocilium (Fig. 1 C), well under the ∼400 actin filaments per mouse utricle stereocilium (Krey et al., 2016). The capping protein subunits are at similar concentrations in isolated hair bundles and whole epithelium (Table S1); given that bundles account for <1% of the total protein in chick or mouse utricles (Krey et al., 2015), the vast majority of CAPZA and CAPZB is present in somas of hair cells and supporting cells.

To compare expression of actin cappers in hair cells with that in other cells of the developing inner ear, we used FACS to sort utricular or cochlear cells from mice expressing *Gfp-Pou4f3* (Masuda et al., 2011; Scheffer et al., 2015; Hickox et al., 2017), which is expressed exclusively in hair cells, and data-independent acquisition (DIA) mass spectrometry to measure protein levels (Venable et al., 2004; Egertson et al., 2015). We generated spectral libraries with data-dependent acquisition (DDA; also known as shotgun) mass spectrometry of whole utricles, isolated hair cells, or purified hair bundles, then used these libraries to identify and quantify peptides, using several proteotypic peptides for each protein (Fig. 1 D). The DDA data were also used to quantify proteins in isolated cells (Table S2).

The capping protein subunits CAPZA1, CAPZA2, and CAPZB were all detected by DIA in GFP-positive hair cells; they were also found in GFP-negative cells (Fig. 1 D and Table S2), which in vestibular tissue are largely supporting cells that act as progenitors for hair cells. Interestingly, although individually expressed capping protein subunits have been reported to be unstable (Soeno et al., 1998) and loss of one subunit leads to loss of the other in eukaryotes (Amatruda et al., 1992; Mejillano et al., 2004), the sum of CAPZA1 and CAPZA2 intensity was approximately fivefold greater than that of CAPZB, suggesting that CAPZA subunits can exist outside of a heterodimer. TWF2 and EPS8L2 were highly enriched in hair cells; because the spectral library contained no peptides for EPS8, its contribution could not be estimated. GSN was present at particularly high levels in P7 utricle hair cells, which was consistent with the high protein levels seen in isolated hair bundles (Fig. 1, B and C). The DDA data gave similar results (Table S2).

Locations of actin cappers in mouse stereocilia

To localize actin cappers in stereocilia, we used conventional confocal microscopy or, for increased resolution, image-scanning microscopy with an Airyscan detector (Müller and Enderlein, 2010; Sheppard et al., 2013; Roth et al., 2016). We used an antibody against CAPZB2 that has been validated with knockdown (Sinnar et al., 2014) and peptide-blocking experiments (Fig. S1, A–D). In both cochlea and utricle, CAPZB2 was detected along stereocilia in a punctate pattern, similar to CAPZB2 labeling in filopodia (Sinnar et al., 2014). In postnatal day 1 (P1) cochlea, sporadic CAPZB2 staining was observed in stereocilia, but more was found near apical surfaces of hair cells (Fig. 2 A). In P8 cochlea, some CAPZB2 was found at stereocilia tips of both inner and outer hair cells, but more labeling was observed along the sides of stereocilia shafts (Fig. 2 A). Punctate labeling was also seen in the somas of hair cells and supporting cells (Fig. 2 A). By P22, less CAPZB2 was detectable in bundles of cochlear hair cells, but it was concentrated at the tips of the second row of stereocilia (Fig. 2 M).

In P1 utricle, CAPZB2 was present in the upper regions of stereocilia in many hair bundles (Fig. 2 B). In P8 utricle, CAPZB2 was present at low levels in the tallest bundles, which are presumably relatively mature; by contrast, CAPZB levels in P8 hair cells were much higher in bundles of intermediate size (Fig. 2, B, P, and Q, arrows). The smallest P8 bundles had little CAPZB2 (Fig. 2 Q, asterisks). CAPZB2 was also present near apical surfaces of supporting cells, presumably in their microvilli (Fig. 2 P, asterisks). By P22, CAPZB2 levels had declined in all utricle bundles (Fig. 2, B and Q). To measure the density of CAPZB in hair bundles, we used average-projected z-stacks and determined the CAPZB2/actin fluorescence intensity ratio for bundles at P1, P8, and P22 (Fig. 2, Q and R). CAPZB2

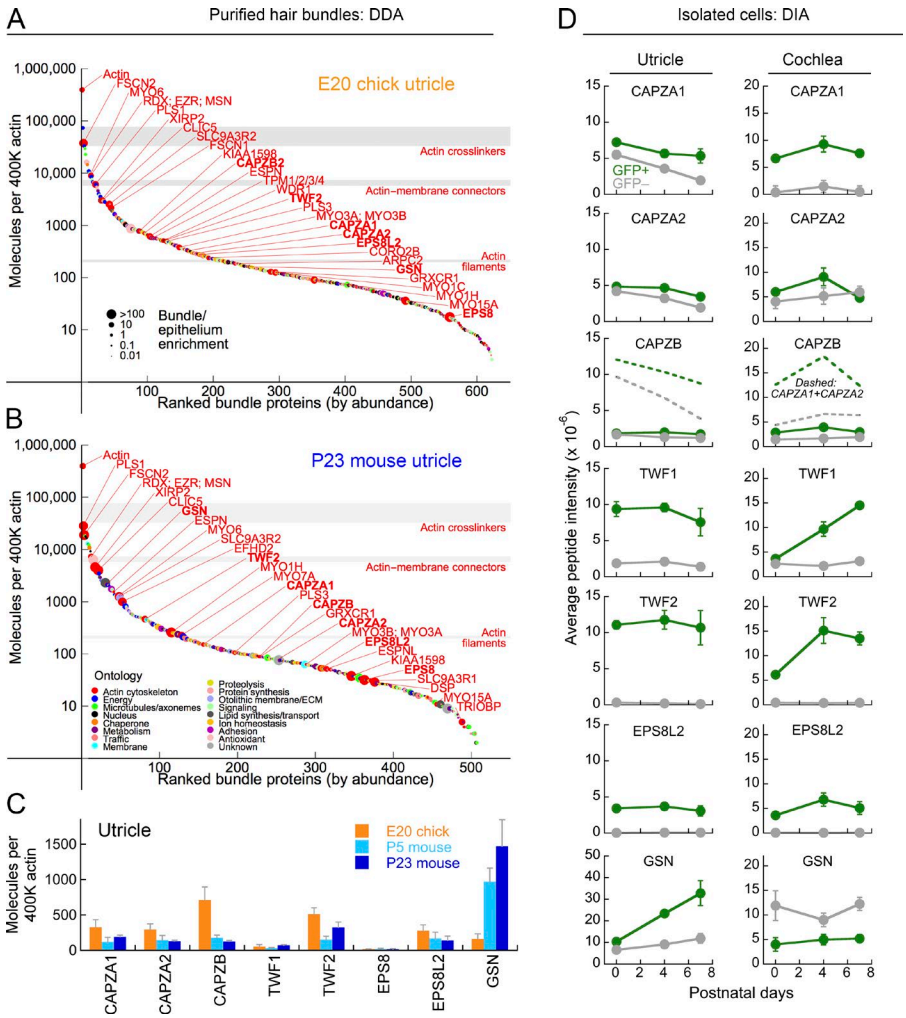

Figure 1. **Mass spectrometry identification and quantitation of hair-bundle actin cappers in chick and mouse inner ear.** (A) Data-dependent acquisition (DDA) mass spectrometry of E20 chick hair bundle proteins detected in three out of three chick datasets. Actin-associated proteins enriched twofold or more in bundles are indicated by red callouts; bold red callouts indicate actin cappers. Bars for actin cross-linkers, actin-membrane connectors, and actin filaments indicate the approximate number of each per stereocilium. (B) DDA analysis of P23 mouse bundle proteins detected in four out of four biological replicates. (C) Capper levels in chick and mouse stereocilia estimated by DDA mass spectrometry. Mean ± SD, $n = 4$ for all. (D) DIA mass spectrometry of isolated cells at different developmental ages. Utricle and cochlea cells were separately isolated by FACS from *Pou4f3-GFP* mice; hair cells are GFP positive (GFP+), and all other cells are GFP negative (GFP–). Dashed lines in the CAPZB panels indicate the sum of the CAPZA1 and CAPZA2 mean peptide intensities. Note y axis expansion for GSN in utricle. Mean ± SD, $n = 3$ for all.

density increased from zero in the smallest bundles to a peak for bundles of ~5 µm in length; as bundles elongated further, the CAPZB2 density declined (Fig. 2 R).

We also localized other actin cappers in hair cells (Fig. 2, C–L). CAPZA1 was located in cochlear and utricular stereocilia in spatial and developmental patterns similar to those of CAPZB2 (Fig. 2, C and D). The distribution of EPS8 and EPS8L2 was similar to that reported previously (Zampini et al., 2011; Furness et al., 2013); EPS8 was detected in hair bundles primarily in the very tallest stereocilia (Fig. 2, E and F, arrows), whereas EPS8L2 was found at the tips of shorter stereocilia (Fig. 2, G–H, arrows). GSN was not detected in P1 or P8 stereocilia, although it was present in some hair cell bodies at high levels (Fig. 2, I and J); at P21, it was occasionally seen at utricle stereocilia tips (Fig. 2 J, asterisks), coinciding with its reported location in cochlea (Mburu et al., 2010; Olt et al., 2014). Finally, similar to a previous study (Peng et al., 2009), TWF2 was located at stereocilia tips, with the highest concentration at the tips of all but the tallest stereocilia (Fig. 2, K–N). At P8, labeling appeared to be associated more with the ankle-link region than tips in the cochlea (Fig. 2 K, arrow), whereas labeling was present both at tips and the ankle region in P8 utricle bundles (Fig. 2 L, asterisks). In P22 cochlea, TWF2 labeling was confined to row 2 stereocilia tips, especially visible in inner hair cells (Fig. 2 N). In utricle, TWF2 immunoreactive punctae were often colocalized with CAPZB2 punctae (Fig. 2 O, arrows).

CAPZB interacts with twinfilins in stereocilia

Colocalization of CAPZB2 and TWF2 (Fig. 2 O), along with previous studies showing that capping protein binds to twinfilins (Palmgren et al., 2001; Vartiainen et al., 2003), suggested that these proteins may physically associate in stereocilia. To identify protein complexes in stereocilia, we immunoprecipitated capping protein from extracts of partially purified stereocilia. We used monoclonal antibodies that recognized mouse CAPZA and CAPZB subunits (Schafer et al., 1996; Fig. 3). When we analyzed immunoprecipitates by either immunoblotting (Fig. 3, A–C) or quantitative mass spectrometry (Fig. 3, D and E), we found that the subunit targeted by the monoclonal antibody was specifically precipitated. Only a fraction of the nontargeted subunit was pulled down in each experiment, however, suggesting again that not all capping protein subunits are present in heterodimers. As in isolated cells, the amount of total CAPZA subunits was approximately five times greater than that of CAPZB subunits in the solubilized stereocilia extract (Fig. 3, D and E; and Table S3). These results were qualitatively replicated by immunoblot analysis of immunoprecipitations from chick ear (Fig. S2 A).

By mass spectrometry analysis, the two most enriched proteins after CAPZB in the mAb 3F2.3 immunoprecipitations (which targeted CAPZB2) were the twinfilins TWF2 and TWF1, which is consistent with our localization experiments.

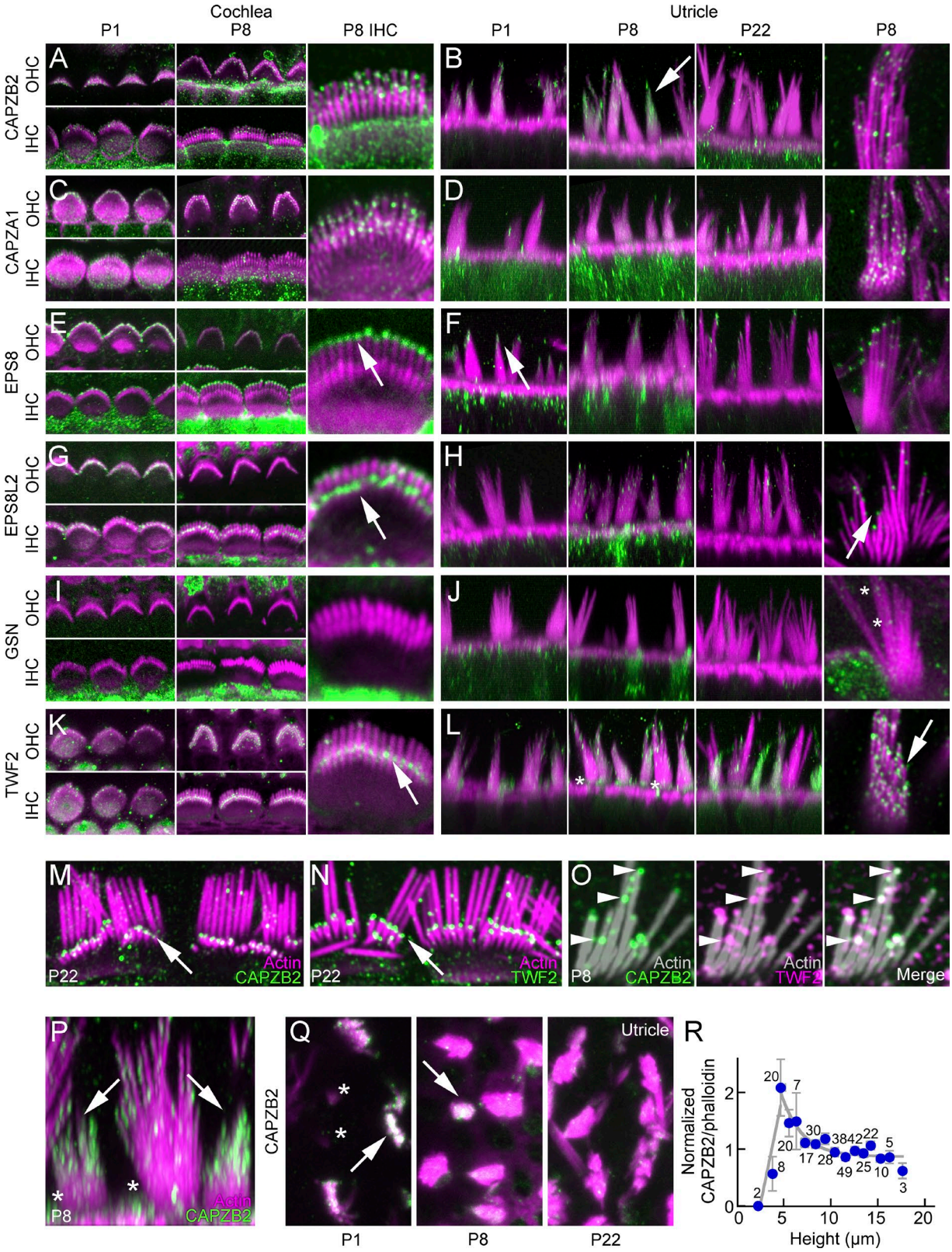

Figure 2. **Actin cappers during postnatal mouse cochlea and utricle development.** (A–L) Localization of actin cappers during development. Primary antibodies are indicated on the left, and developmental age and organ on the top. (A) CAPZB2 in cochlea. (B) CAPZB2 in utricle. Arrow indicates medium-sized hair bundle with strong CAPZB2 labeling. (C) CAPZA1 in cochlea. (D) CAPZA1 in utricle. (E) EPS8 in cochlea. Arrow indicates strong labeling at tips of row 1 (tallest) inner hair cell (IHC) stereocilia. (F) EPS8 in utricle. Arrow indicates labeling at tips of tallest stereocilia. (G) EPS8L2 in cochlea. Arrow indicates strong labeling at tips of row 2 inner hair cell stereocilia, although row 1 stereocilia are also labeled. (H) EPS8L2 in utricle. Arrow indicates labeling of tips of intermediate-length stereocilia. (I) GSN in cochlea. (J) GSN in utricle. Asterisk indicates occasional tip labeling in utricle bundles. (K) TWF2 in cochlea. Labeling in inner hair cells is similar to that of ankle links (arrow) rather than stereocilia tips. (L) TWF2 in utricle. Labeling at stereocilia tips is strong

By contrast, neither twinfilin was immunoprecipitated with mAb 5B12.3, which recognizes CAPZA1 and CAPZA2 (Fig. 3 F). Twinfilins were each present in the stereocilia extract at ∼10% the concentration of CAPZB (Fig. 3 E and Table S3).

Unexpectedly, mAb 5B12.3 also precipitated the mitochondrial pyruvate dehydrogenase (PDH) complex (Fig. 3, D and F). Because PDH subunits were also enriched in the mAb 3F2.3 immunoprecipitates (Fig. 3 F), the complex apparently interacts directly with capping protein rather than binding to the precipitating antibody. We noted that PDK1 and PDK3, members of the PDH complex (Patel et al., 2014), contain a match to the capping-protein interaction motif (Edwards et al., 2014; Fig. S2 B). Small amounts of CAPZA1/2 or CAPZB2 were coprecipitated with the PDH E2 subunit (Fig. S2, C and D). The significance of the capping protein–PDH interaction is unclear.

Auditory and vestibular function in mice lacking *Capzb*

To examine the functional role of capping protein in stereocilia function, we generated *Capzb* knockout mice; although there are three *Capza* genes, the single *Capzb* gene expresses both *Capzb* splice forms. Because deletion of the *Capzb* gene is embryonic lethal (White et al., 2013), is expressed in inner-ear supporting cells, and may be expressed in progenitors (Fig. 1 D), we confined the effect of *Capzb* deletion to hair cells by using a floxed *Capzb* allele and the *Atoh1-Cre* mouse line (Matei et al., 2005).

In *Capzb$^{fl/fl}$;Atoh1-Cre* mice, which we refer to as *Capzb^{CKO}*, auditory function at P120, as assessed by auditory brainstem response (ABR) and distortion-product otoacoustic emission (DPOAE) measurements, was profoundly diminished (Fig. 4). ABR thresholds were elevated to the instrument sensitivity level (Fig. 4, A and B), and DPOAEs were at the noise floor (Fig. 4, C and D). Vestibular function was strongly reduced as well. Although the mice did not show overt circling behavior, they exhibited a "shaker" phenotype that became progressively worse after weaning (Video 1); moreover, vestibular-evoked potential (VsEP) thresholds were dramatically elevated, with only one of five mice showing any detectable VsEP (Fig. 4, E and F). Responses in heterozygous mice were similar to those in wild types for ABRs, DPOAEs, and VsEPs (Fig. 4). CAPZB is thus necessary for auditory and vestibular function.

Morphology of auditory hair cells lacking *Capzb*

Loss of auditory function suggested that cochlear hair cells were affected by *Capzb* deletion. To examine how hair cells change morphologically as CAPZB disappeared, we generated *Capzb^{CKO};Ai14* mice (Fig. 5, A and B); tdTomato expression in these mice reports CRE expression (Madisen et al., 2010). The phenotype of *Capzb^{CKO}* hair cells included disappearance of distinguishable stereocilia (Fig. 5 B, number signs), ruptures in cuticular plates (Fig. 5 B, arrows), increased actin aggregation in the adherens-junction region (Fig. 5, B and D, arrowheads), and expansion of the apical surface (Fig. 5 B, dashed box). These changes appeared to develop together, so that a hair cell with shortened or missing stereocilia had very apparent changes in actin of the cuticular plate and adherens junctions.

When examining *Capzb^{CKO}* cochleas labeled with anti-CAPZB2, we noted that in comparison to control cochleas (Fig. 5 C), CAPZB2 was diminished in cell bodies of hair cells, although not always in their stereocilia (Fig. 5, D and F); the degree of bundle degeneration was, however, roughly inversely correlated with the amount of bundle CAPZB2 (Fig. 5, D and F). Even in the same bundle, however, stereocilia apparently disappeared at different rates, as stereocilia were less uniform in length in the same row (Fig. 5, D and F). By contrast, stereocilia in the same row were roughly the same height in control hair cells (Fig. 5, C and E).

To better visualize changes in stereocilia dimensions, we used scanning electron microscopy to examine hair bundles of *Capzb^{CKO}* mice. In the cochlear apex, which develops more slowly than the base, bundles in control and *Capzb^{CKO}* mice were comparable at P1 (Fig. S4, A–F). Although most bundles from basal hair cells also looked normal, some hair cells showed disarray of their stereocilia (Fig. S4, C–F). By P4, a greater number of basal bundles were affected; some bundles had mild orientation or shape disruption, whereas other bundles were composed of short, narrow stereocilia of similar length arranged in a circular or fragmented pattern (Fig. 5, G and H). At this age, CAPZB2 expression resembled that at P8 (Fig. S4 G). Stereocilia width was decreased in *Capzb^{CKO}* inner hair cells, even if their bundles looked relatively normal in organization (Fig. 5 Hii, asterisks). Cell-to-cell variability of the phenotype in light and electron microscopy presumably reflected differences in timing of the loss of CAPZB; indeed, very few bundles remained at P21, and none appeared normal (Fig. 5 I). Stereocilia rootlet remnants near apical surfaces suggested that hair cells lost their bundles but did not degenerate. The principal phenotype in *Capzb^{CKO}* cochleas was thus the reduction in stereocilia diameter and length, with eventual disappearance of most bundles.

Morphology of vestibular hair cells lacking *Capzb*

Consistent with VsEP threshold elevation, vestibular hair cells were also affected by loss of *Capzb*. Low-magnification views of *Capzb^{CKO};Ai14* utricles at P21 showed that the number of normal hair bundles was substantially reduced, and some cells appeared to be undergoing extrusion from the epithelium (Fig. 6, A and B). Morphological changes in *Capzb^{CKO}*

at P8; labeling near ankle links is also apparent (asterisks). (M) CAPZB2 labeling in P22 apical cochlea inner hair cells. Arrow indicates strong labeling at row 2 tips. (N) TWF2 labeling in P22 apical cochlea inner hair cells. Arrow indicates strong labeling at row 2 tips. (O) Double labeling of CAPZB2 (green) and TWF2 (magenta). Green and magenta channels were subjected to two-pixel Gaussian filtering. Arrowheads indicate several coincident green and magenta spots. (P) High-magnification view (projected x-z reslices) of increased CAPZB2 labeling density in short utricle bundles (arrows). Asterisks indicate labeling at supporting cell apical surfaces. (Q) CAPZB2 density in bundles during development. Confocal images (averaged z-planes) showing no labeling in small bundles (asterisks), strong labeling in medium-sized bundles (arrows), and reduced labeling in tall bundles. (R) Relation between bundle height (in tranches of 1 µm) and CAPZB2/phalloidin ratio. Gray line is exponential rise for the first three points, exponential fall for remaining points. Mean ± SEM is plotted; number of bundles measured (n) for each height tranche is indicated. Panel full widths are as follows: In A, C, E, G, and I, low-power outer hair cell (OHC) and inner hair cell panels are 25 µm wide, and the high-magnification inner hair cell image is 8 µm wide. In B, D, F, H, and J, the left three panels are maximum projections of 10-µm-deep x-z reslices, taken from z-series, and are 25 µm wide; high-magnification panels on the right are 8 µm wide. In K and L, panels are 20 µm wide. In M, panels are 7 µm wide. In N, the panel is 14.5 µm wide. In O, panels are 25 µm wide. All high-magnification panels used maximum projection of several z-sections (not x-z reslices) from images acquired with Airyscan detector.

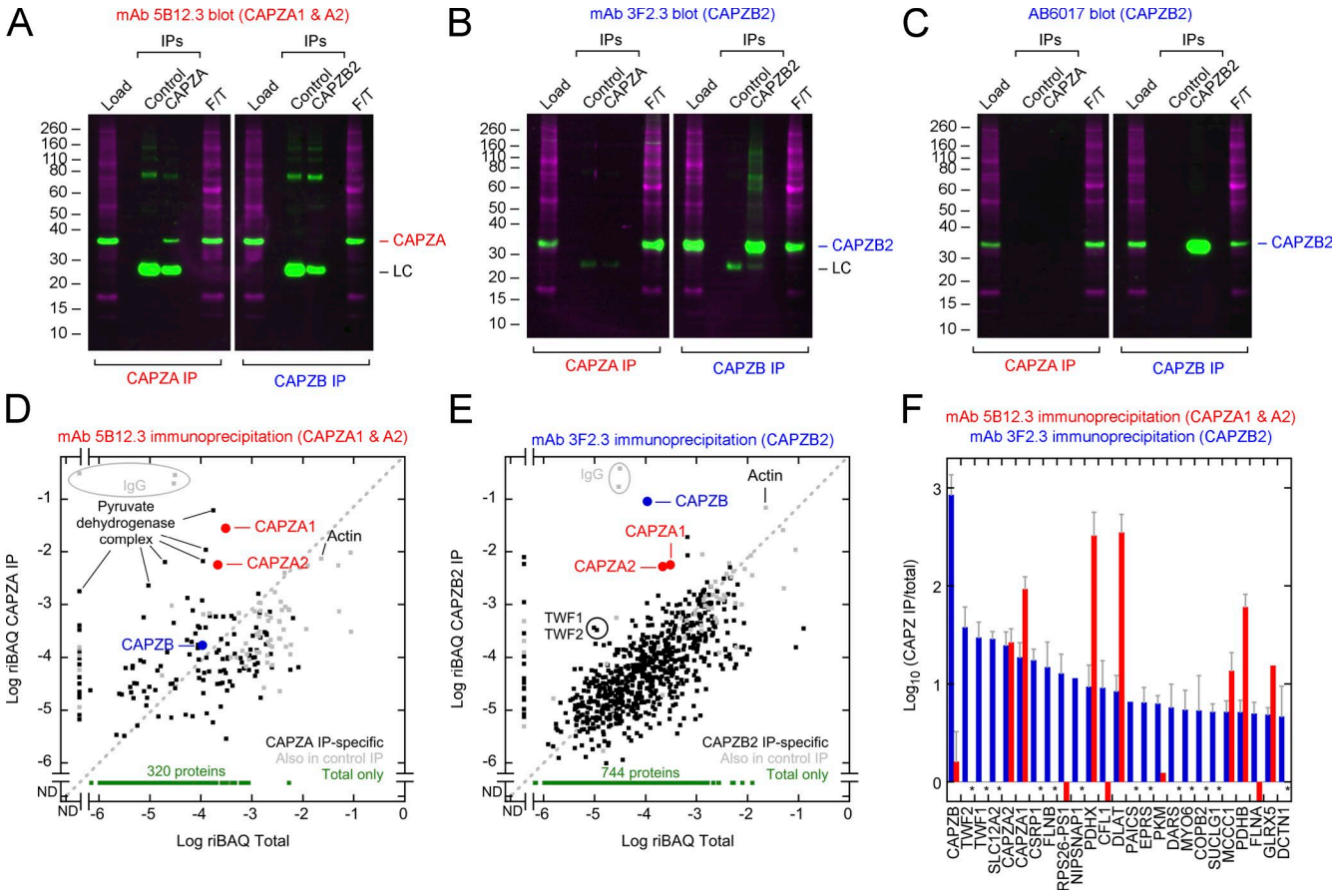

Figure 3. **Immunoprecipitation of capping protein from mouse crude stereocilia extracts.** Crude mouse stereocilia were solubilized with RIPA buffer and then subject to sequential control and CAPZ subunit immunoprecipitations. (A–C) Immunoblot analysis. Total and flow-through (F/T) samples are loaded at 33%; immunoprecipitates are loaded at 100%. (D and E) Quantitative mass spectrometry analysis comparing each protein's relative abundance (riBAQ) in the total sample (x axis) and the specific immunoprecipitate (y axis). Capping protein subunits, contaminating immunoglobulins (IgG), and actin are indicated in each plot. In CAPZA immunoprecipitates, large amounts of multiple subunits of the PDH complex were observed (D). In CAPZB2 immunoprecipitates, twinfilins TWF1 and TWF2 were each substantially enriched (indicated by vertical distance from dashed gray unity line). Only proteins detected in two out of three total replicates or two out of two immunoprecipitation replicates are plotted. ND, not detected. (F) Immunoprecipitate/total riBAQ ratio for the 25 most-enriched proteins in the CAPZB2 immunoprecipitations; note log scale. riBAQ ratios for CAPZA immunoprecipitates are also indicated. Mean ± SD is plotted, $n = 2$. Asterisks indicate not detected in CAPZA immunoprecipitations.

utricle hair cells were somewhat different from those in cochlear hair cells. Using light microscopy or scanning electron microscopy at P2, when most hair cells are less than 1 wk old, wild-type and *Capzb*^{CKO} hair cells could not be easily distinguished (Fig. 6, C and D). By P7–P9, however, there was a mix of bundle phenotypes (Fig. 6, E and F). Some bundles appeared to be highly disrupted; a common phenotype was of a bundle missing many of its shortest stereocilia but still possessing some stereocilia of intermediate length (Fig. 6, F, L, and N). Other bundles in *Capzb*^{CKO} utricles appeared to be completely normal, however, but may have arisen from relatively newly formed hair cells.

Other phenotypes were obvious at P7–P9 as well. Cuticular plates appeared to be hollowed out, with a central hole, whereas circumferential actin belts had expanded (Fig. 6, E and F). In addition, large actin aggregates were present in the basal cytoplasm of hair cells with disheveled or missing hair bundles (Fig. 6, F and P). These aggregates, which resemble cytocauds (Kanzaki et al., 2002), also costained for ESPN, an abundant bundle actin cross-linker (Fig. 6 P); the expanded actin belts had significantly lower ESPN immunoreactivity than stereocilia, however. In the cochlea, we saw the cytocaud-like actin aggregates in a few inner hair cells as well, although rarely in outer hair cells.

By P15, very few bundles appeared normal; many were <5 µm tall (Fig. 6, G and H). Disrupted cuticular plates and expanded circumferential actin belts were seen in nearly all cells. At ∼P100, we observed MYO7A-positive cells in *Capzb*^{CKO} utricles; most contained long kinocilia but a small or absent bundle (Fig. 6 J, arrow). The density of MYO7A-positive cells was considerably lower in *Capzb*^{CKO} utricles than in control utricles (Fig. 6, I and J), and those cells appeared to be enlarged. Some normal-appearing bundles were present as well (Fig. 6 J, asterisk); these might have been on newly formed hair cells, as hair cell turnover continues in adult mouse utricles (Bucks et al., 2017). These hair cells may be responsible for the very limited vestibular function measured with *Capzb*^{CKO} mice (Fig. 4, E and F).

As with cochlear hair cells, CAPZB2 staining disappeared from somas of *Capzb*^{CKO} utricle hair cells before it did from stereocilia (Fig. 6 M, asterisks). Anti-CAPZB2 still labeled many stereocilia, but not the very shortest ones (Fig. 6 M, arrow); by contrast, anti-ESPN labeled all stereocilia, including the shortest ones (Fig. 6 O). We also examined utricle stereocilia

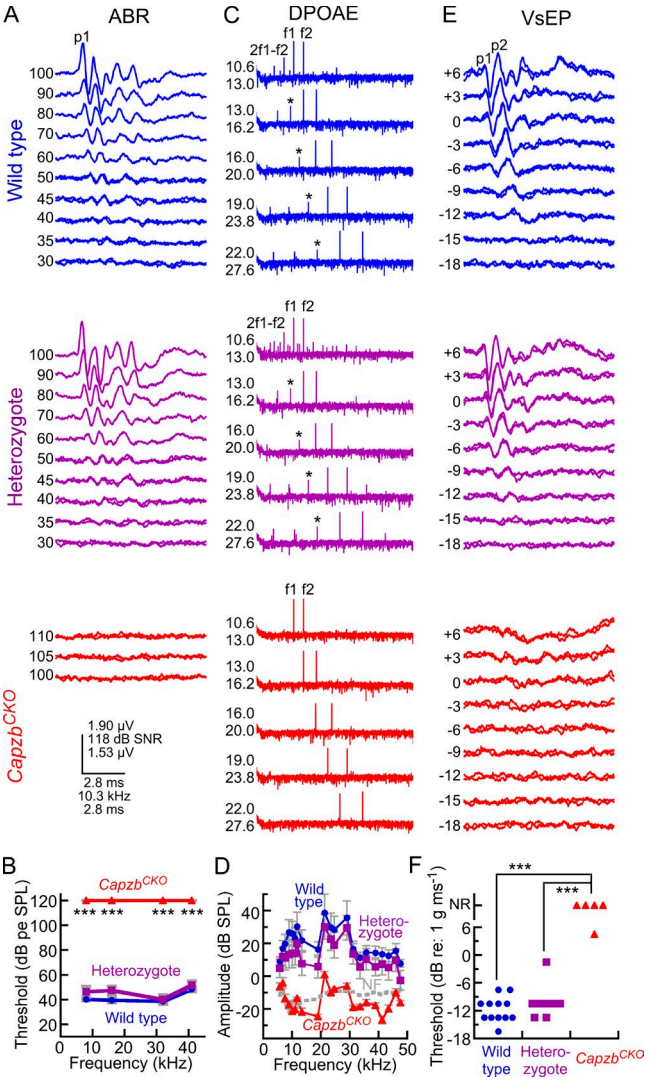

Figure 4. **Effects of *Capzb* deletion on auditory and vestibular function.** (A and B) Auditory brainstem response (ABR). (A) Waveform examples at indicated decibel sound pressure level at 8 kHz for wild-type, heterozygous, and *Capzb*^{CKO} mice are at top. (B) Summarized data (mean ± SEM). (C and D) Distortion-product otoacoustic emissions (DPOAE). (C) Waveform examples for indicated f1 and f2 primaries and the 2f1-f2 distortion product (asterisks) for wild-type, heterozygous, and *Capzb*^{CKO} mice. (D) Summarized data (mean ± SEM). (E and F) Vestibular evoked potentials (VsEPs). (E) Waveform examples in response to linear jerk pulses at indicated stimulus level for wild-type, heterozygous, and *Capzb*^{CKO} mice. (F) Summarized data (mean ± SEM). Calibration bars represent amplitudes in microvolts for ABR, decibel signal-to-noise ratio (dB SNR) for DPOAE, and microvolts for VsEP. Time is represented in milliseconds for ABR and VsEP waveforms. Frequency for DPOAE waveforms is represented in kilohertz. ***, P < 0.001.

isolated on glass and visualized with image-scanning microscopy. By P23, strong labeling for CAPZB2 was observed at stereocilia tips, particularly on short-to-medium length, wide stereocilia (Fig. 6 Q, arrows). Some staining was still observed in *Capzb*^{CKO} hair cells at P23 (Fig. 6 R), but it was considerably less than in controls.

Scanning electron microscopy at P25 (Fig. 6, K and L) confirmed that almost all bundles were abnormal; most small bundles had tall kinocilia, suggesting those hair cells had differentiated earlier in development. Moreover, the relatively short height of kinocilia associated with normal-appearing bundles indicated that those cells were recently differentiated. Finally, other cells had smooth apical surfaces with what appeared to be stereocilia rootlet remnants, similar to what was seen in the cochlea. CAPZB thus appears to be required for utricle stereocilia maintenance.

Stereocilia length and width are decreased in *Capzb*^{CKO} utricles

Using image-scanning microscopy, we measured key structural parameters of control and *Capzb*^{CKO}*;Ai14* hair cells in whole mounts of P21 utricles (Fig. 7, A–M). The tallest stereocilia were significantly shorter in *Capzb*^{CKO} hair cells (Fig. 7 K), but kinocilium heights were only modestly reduced (Fig. 7 L). Individual stereocilia were narrower in *Capzb*^{CKO} hair cells (Fig. 7 H); although the cross-sectional area of the hair bundle was reduced (Fig. 7 F), the number of stereocilia was unchanged in most bundles (Fig. 7 E), consistent with the decreased diameter. The cross-sectional area of apical regions of *Capzb*^{CKO} hair cells expanded substantially as well (Fig. 7 G). The mean tdTomato signal was higher in *Capzb*^{CKO} hair cells than in controls and was inversely proportional to the stereocilia diameter (Fig. 7 J). If the tdTomato signal is a proxy for the age of *Capzb*^{CKO} hair cells, the data in Fig. 7 J suggest that stereocilia diameter is normal initially but then decreases as CAPZB is lost.

We also estimated the properties of the hair-bundle bevel by counting the number of stereocilia at successive heights above the cell apex (Fig. 7 M). Using number of stereocilia to represent lateral distance in the bundle, we noted that *Capzb*^{CKO} stereocilia were shorter across the bundle bevel, as if they all shortened the same distance (Fig. 7 M). A few bundles from *Capzb*^{CKO} utricles were ~5 µm tall; most had <20 stereocilia each, consistent with all rows of stereocilia disappearing by the same distance so that the shortest rows disappeared (Fig. 7 M, red asterisk).

We also examined the length and width of isolated stereocilia from wild-type and *Capzb*^{CKO} utricles (Fig. 7, N–U). Although relationships between stereocilia are lost, dimensions can be measured with greater accuracy than from whole mounts. At P8, there was only a slight difference in the length distribution of stereocilia from wild-type and *Capzb*^{CKO} utricles (Fig. 7 R; Student's *t* test, P = 0.003). By P25, however, many more short *Capzb*^{CKO} stereocilia were seen and far fewer longer ones were present as compared with wild type (Fig. 7 S; P = 10^{-35}). *Capzb*^{CKO} stereocilia were slightly narrower than wild type at P8 (Fig. 7 T); P8 wild-type stereocilia were 399 ± 71 nm in diameter (mean ± SD; *n* = 1,100), whereas *Capzb*^{CKO} stereocilia were 377 ± 74 nm (*n* = 986; P = 10^{-11}). By contrast, *Capzb*^{CKO} stereocilia were much narrower at P25 (Fig. 7 U); wild-type stereocilia were 381 ± 66 nm in diameter (*n* = 388), whereas *Capzb*^{CKO} stereocilia were 307 ± 55 nm (*n* = 393; P = 10^{-55}). These results also showed that *Capzb*^{CKO} stereocilia were initially of normal length and diameter but then shrank in both dimensions as the hair cell aged.

In utero delivery of MYC-CAPZB2 affects stereocilia length and diameter

We sought to manipulate stereocilia length and width using exogenous capping protein constructs; previous studies reported that expression of CAPZB alone modulates actin dynamics in cells (Jo et al., 2015). Using in utero electroporation to deliver expression constructs between embryonic day 11 (E11) and E12 and analyzing at P2, we found that GFP-CAPZB2 targeted

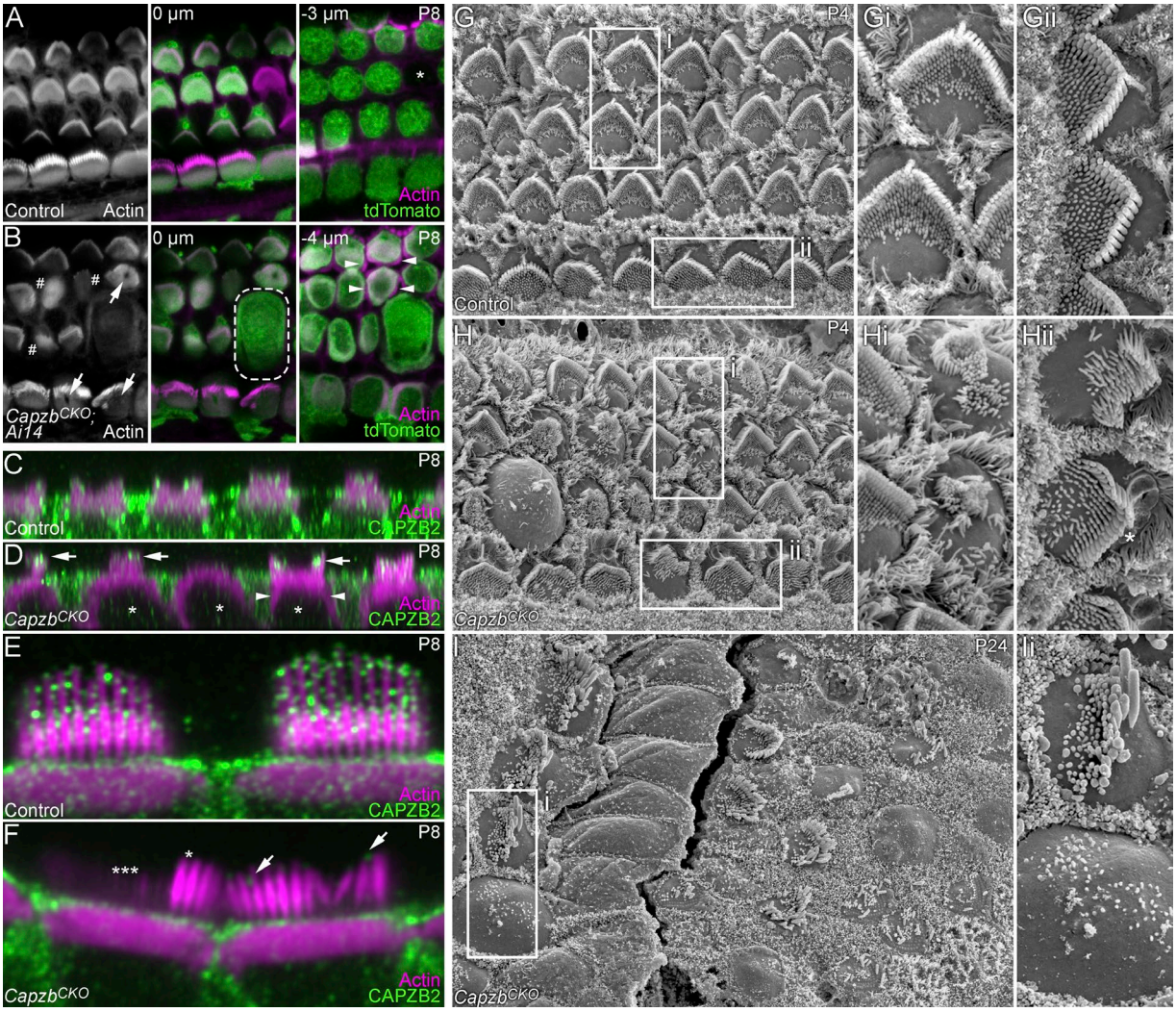

Figure 5. **Consequences of *Capzb* deletion in cochlea.** (A and B) Bundle and cell morphology in *Capzb*^{CKO}*;Ai14* cochlea. Occasional hair cells (<1%) were Ai14 negative (*). Several phenotypes of *Capzb*^{CKO} hair cells are indicated in B: cells with no stereocilia (#), ruptures in cuticular plates (arrows), increased actin density in adherens junction region (arrowheads), and expanded cross-sectional area of hair cell (dashed box). (C and D) Reslice of z-stack through outer hair cells showing that CAPZB2 immunolabeling is diminished in hair cell somas of *Capzb*^{CKO} mice (asterisks), but some immunoreactivity remains in stereocilia (arrows). Arrowheads indicate increased actin density in adherens junction region. (E and F) High-magnification views of anti-CAPZB2 staining of control (E) and *Capzb*^{CKO} (F) inner-hair cell bundles; panels are 18 µm wide. z-projection of 1.5 µm completely through the bundles displayed. In F, some residual CAPZB2 immunoreactivity is apparent in tall stereocilia (arrow). Note too that the bundle on the left has a region where stereocilia are near normal length (*) and another region where stereocilia have shortened and thinned (***). (G–I) Scanning electron microscopy of control (G) and *Capzb*^{CKO} (H and I) cochleas. G and H are 45 µm wide, whereas panel I is 60 µm wide; all insets are 8 µm wide.

to cochlear stereocilia, with evident enrichment near stereocilia tips of cochlear hair cells (Fig. S5 A). After transfection with either MYC-tagged CAPZB2 or CAPZA1, as well as ZsGreen expressed from the same plasmid, we found that ZsGreen-positive inner or outer hair cells at P6 were very similar to untransfected control cells in the same epithelium (Fig. S5, B and C). There was no detectable change in stereocilia length or diameter when either MYC-CAPZB2 or MYC-CAPZA1 was expressed in cochlear hair cells (Fig. S5, B and C). We also delivered capping protein subunits into cochlear hair cells using injectoporation (Xiong et al., 2014). As with the in utero electroporation experiments, CAPZA1 and CAPZB1 were concentrated in stereocilia, apparently focused toward stereocilia tips (Fig. S5, D and E). No phenotype was seen in hair bundles of transfected cells using confocal microscopy. Expression of single capping protein genes in cochlear hair cells thus has no apparent phenotype.

By contrast, the dimensions of hair bundles of P1 utricle hair cells were profoundly affected by transfection with MYC-CAPZB2. Most bundles arising from transfected hair cells had stereocilia that were short and similar in height (Fig. 8 B), whereas hair cells in untransfected regions of the utricle had bundles of normal heights with the usual staircase arrangement (Fig. 8 A). Control hair cells had a bimodal distribution of bundle height, with populations with bundles of ∼4 µm or ∼9 µm tall (Fig. 8 C); these populations likely arise from the two waves of early hair cell generation in the mouse utricle (Denman-Johnson and Forge, 1999; Géléoc et al., 2004). By contrast, hair cells transfected with the MYC-CAPZB2 were all ∼4 µm tall (Fig. 8 C), suggesting that expression of this construct halts bundle development.

Hair bundles of transfected cells had additional abnormalities. In particular, near the tips, stereocilia appeared to swell

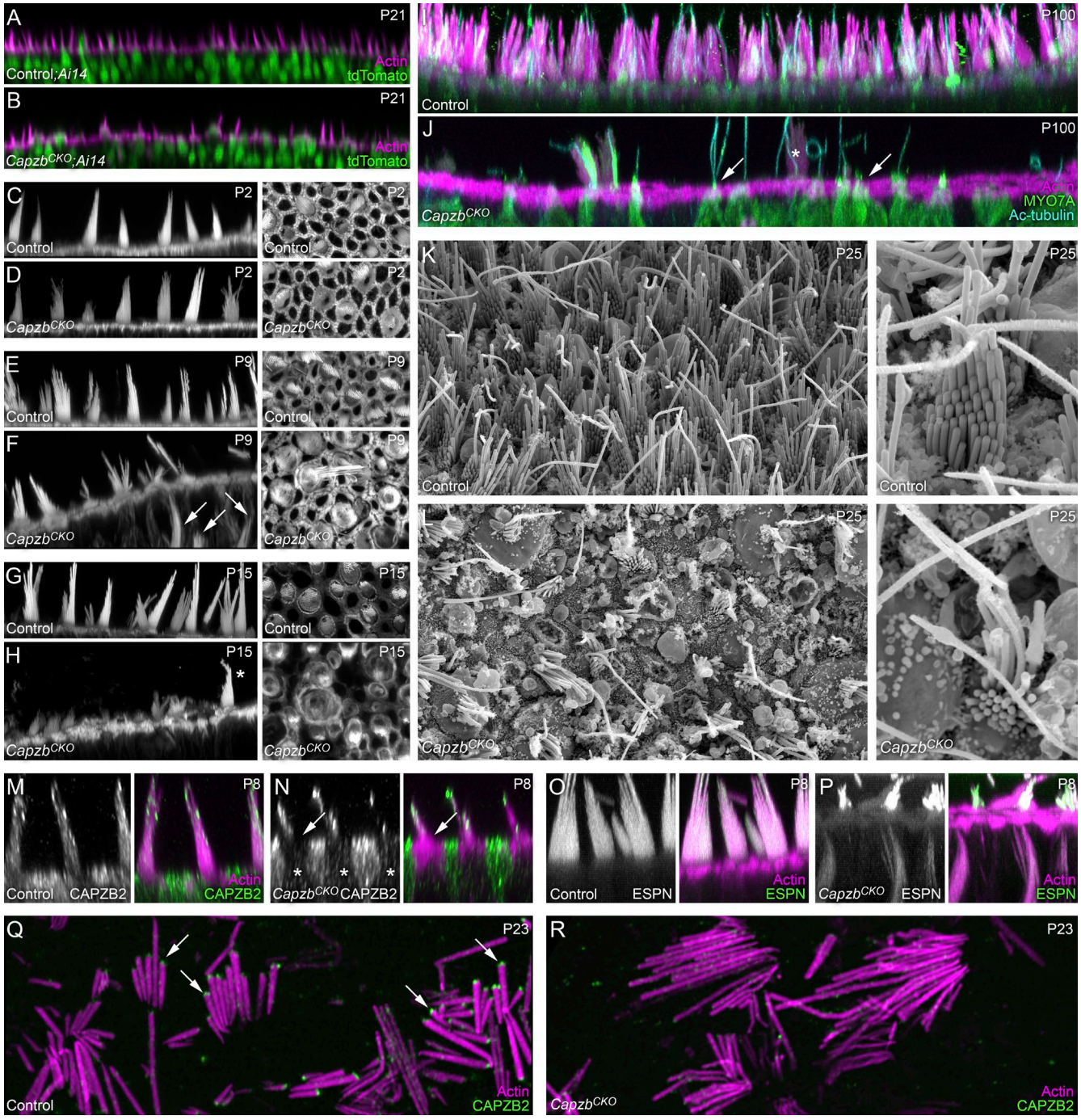

Figure 6. **Consequences of *Capzb* deletion in utricle.** (A and B) Cell morphology in control;*Ai14* and *Capzb*^{CKO};*Ai14* utricular macula at P21 using phalloidin and tdTomato. Note the reduced number of hair bundles and partially extruded cells in *Capzb*^{CKO} utricle. (C–H) Phalloidin staining of bundles (left) and cell apex (right) at indicated developmental times and genotypes. Disruption of cuticular plates in *Capzb*^{CKO} utricles is apparent even at P2. At P9, cytocauds are visible in *Capzb*^{CKO} utricles (arrows). At P15, only occasion normal-appearing bundles are seen in *Capzb*^{CKO} utricles (asterisk). (I and J) Utricle at ~P100. Occasional normal-appearing bundles are seen in *Capzb*^{CKO} utricles (asterisk), but most bundles are very small (arrows), even if they have long kinocilia. (K and L) Scanning electron microscopy of control and *Capzb*^{CKO} utricles. Insets show representative bundles; note that the *Capzb*^{CKO} bundle has very short stereocilia except for the tallest one or two rows. (M and N) CAPZB2 staining of control and *Capzb*^{CKO} utricles. Left panels are CAPZB2 channel alone, right panels have merged phalloidin and CAPZB2 channels. The arrow in N indicates short stereocilia that stained with phalloidin but not anti-CAPZB2; asterisks indicate reduced CAPZB2 staining specifically in hair cell somas. (O and P) Pan-ESPN staining of control and *Capzb*^{CKO} utricles. The left panel is ESPN channel alone, and the right panel has both phalloidin and ESPN channels. Note the prominent cytocauds in the *Capzb*^{CKO} hair cells; they stain with anti-ESPN, albeit less strongly than do bundles. (Q and R) Isolated stereocilia from P23 heterozygous (Q) or *Capzb*^{CKO} (R) utricles. At this age, short and medium-length stereocilia that are relatively thick in diameter have strong CAPZB2 staining at tips (arrows). Panel full widths: (A and B) 300 µm; (C–H) 70 µm (left) and 18 µm (right); (I and J) 150 µm; (K and L) 50 µm (left) and 7.5 µm (right); (M–P) 20 µm; (Q and R) 40 µm.

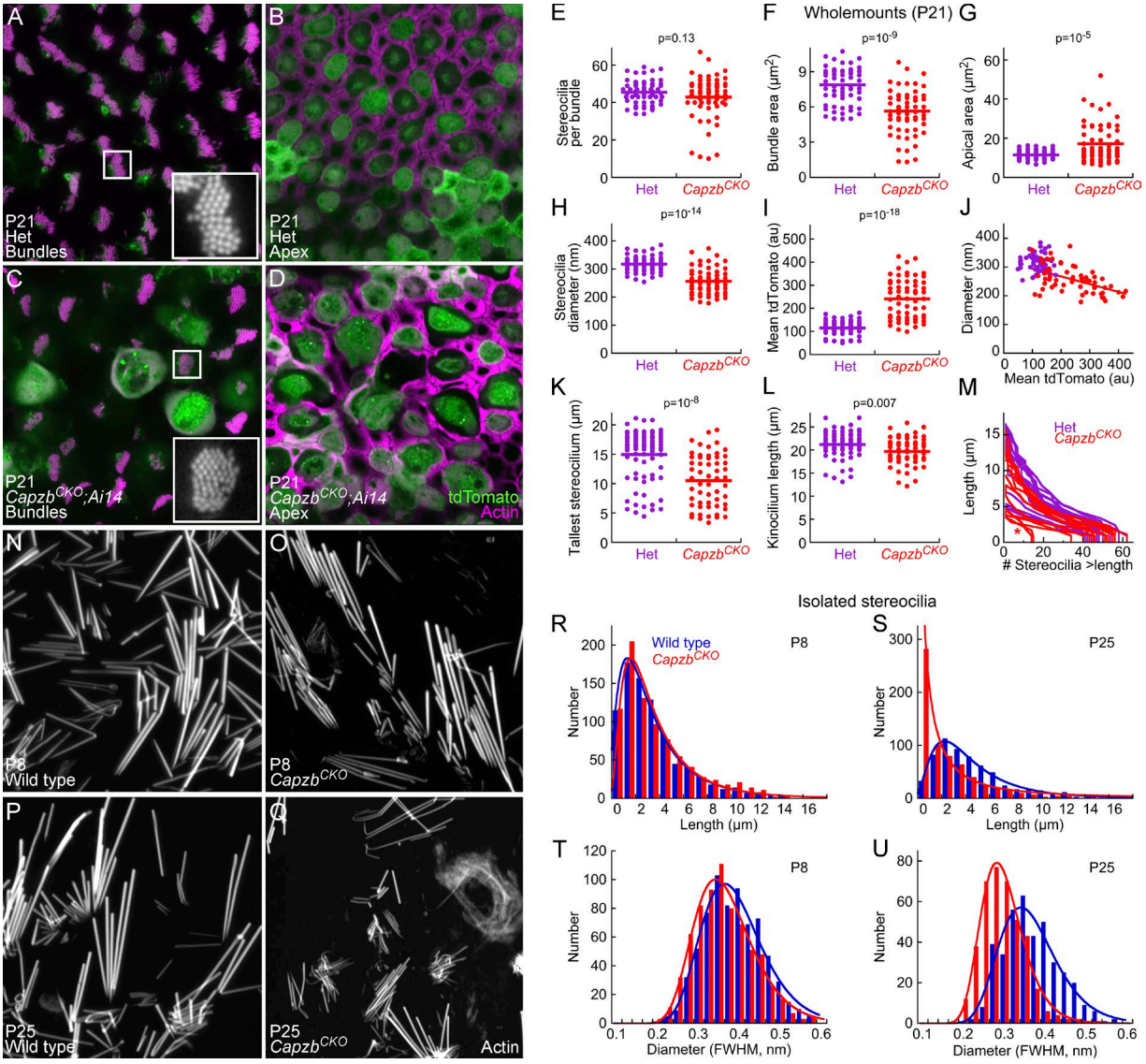

Figure 7. ***Capzb*^{CKO} utricle hair bundles are short and have narrow stereocilia.** (A–D) Confocal slices through hair bundles (A and C) or cell apex (B and D) of heterozygous control (A and B) or *Capzb*^{CKO} utricle. Insets in A and C show representative bundles; the lower intensity of the bundle in C indicates fewer actin filaments and hence a narrower diameter. (E–M) Measurements of hair cell properties from P21 heterozygous and *Capzb*^{CKO} utricles using image-scanning microscopy. (E) Stereocilia per bundle. (F) Cross-sectional area of bundle at base. (G) Cross-sectional area of cell apex. (H) Stereocilia diameter. (I) Mean tdTomato intensity at cell apex. (J) Relationship between stereocilia diameter and tdTomato mean intensity. (K) Length of tallest stereocilia. (L) Length of kinocilium. (M) Profile of bundles; for each height step in a confocal z-stack, the number of stereocilia still present was counted. (N–Q) Isolated stereocilia from P8 and P25 utricles. (R and S) Length distributions for P8 (R) and P25 (S) stereocilia. (T and U) Diameter distributions for P8 (T) and P25 (U) stereocilia; diameter estimated from full width at half-maximum of a Gaussian profile across the stereocilium. Panel full widths: (A–D) 45 µm; (N–Q) 30 µm.

to an abnormally large diameter (~1 µm) or to fuse together (Fig. 8, D and E). These results suggested that whereas MYC-CAPZB2 prevented stereocilia elongation, widening proceeded albeit in an unregulated manner.

To interpret these results, we examined whether CAPZB2 had actin-capping activity on its own (Fig. 8, F–H). We expressed mouse MYC-CAPZB2 in HEK293 cells and purified the protein using 9E10 anti-MYC immunoaffinity chromatography (Agrawal and Schatz, 1997; Geisberg and Struhl, 2004) and gel filtration, which allowed us to remove heterodimers that arose from interaction of CAPZA expressed endogenously by HEK cells and recombinant MYC-CAPZB2. No CAPZA subunits were present in the MYC-CAPZB2 protein preparation (Fig. 8 F). Like CAPZB1 (Remmert et al., 2000), CAPZB2 was stable in the absence of a CAPZA subunit.

We used this MYC-CAPZB2 preparation to interfere with in vitro actin assembly from preformed actin-filament seeds (Kuhn and Pollard, 2007). Mouse CAPZA1/CAPZB2 heterodimer expressed and purified from *Escherichia coli* was a potent inhibitor of actin polymerization (Fig. 8 G). MYC-CAPZB2 slowed filament assembly as well, but only at concentrations ~100-fold greater than the authentic heterodimer (Fig. 8, G and H). As a monomer, MYC-CAPZB2 is unlikely to cap actin filaments in cells, but it could bind to excess endogenous CAPZA subunits to increase the heterodimer concentration.

Stereocilia expression of capping protein regulator PLEKHO1

Proteins containing the capping-protein interaction motif interact with capping protein to recruit it to specific locations and

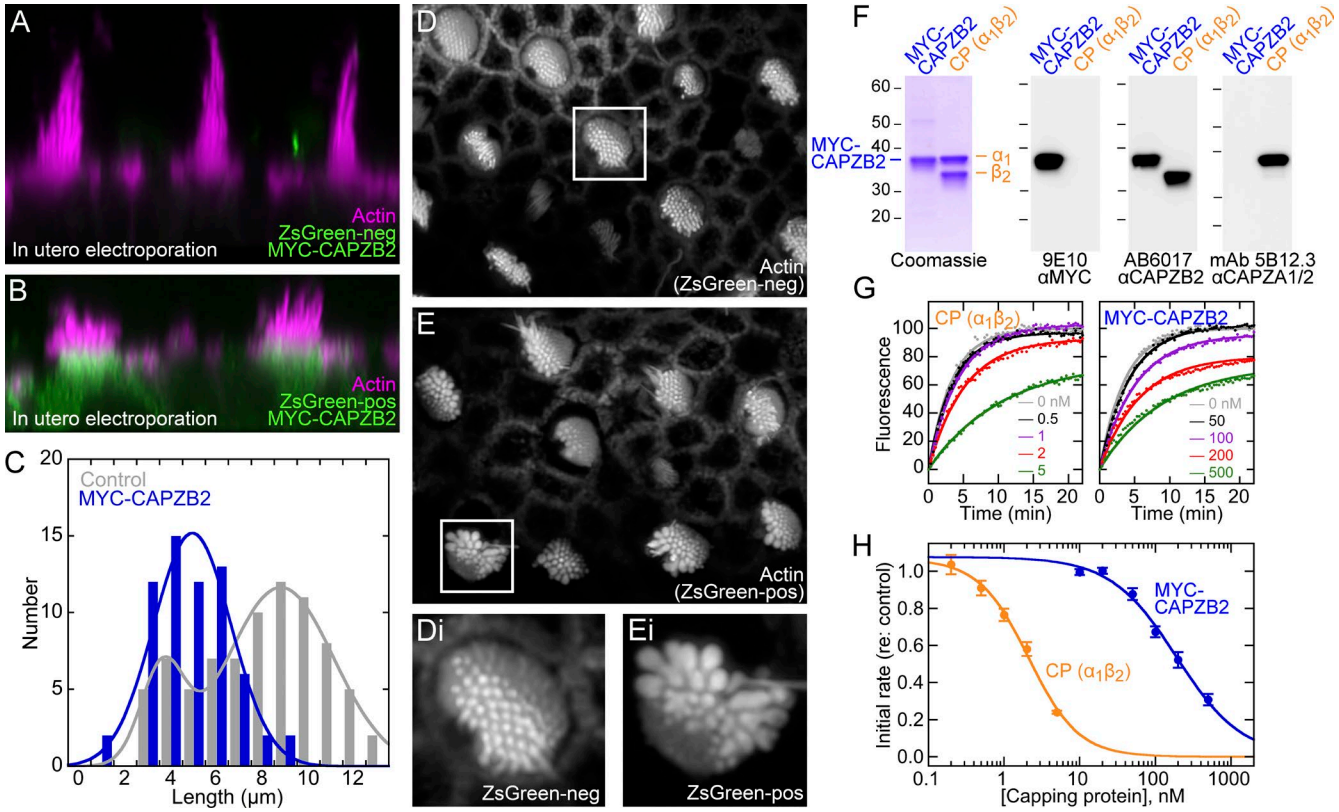

Figure 8. **Heterologous MYC-CAPZB2 disrupts normal utricle stereocilia formation.** (A) Stereocilia morphology in a nontransfected region (no ZsGreen signal) using z-stack reslice. (B) Stereocilia morphology in a transfected region (ZsGreen cell fill) using z-stack reslice. (C) Distribution of tallest stereocilia length of hair bundles from control (untransfected ears plus nontransfected regions) and MYC-CAPZB2–transfected hair cells. Two-Gaussian fits. (D and E) Single z-sections with phalloidin labeling of nontransfected (G) and transfected (H) regions; panels in Di and Ei are magnifications of boxed regions in D and E. Panel full-widths: (A and B) 30 µm; (D and E) 40 µm; (Di and Ei) 7.5 µm. (F) Purification of MYC-CAPZB2 from HEK cells. Left, Coomassie-stained SDS-PAGE gel with purified MYC-CAPZB2 and capping protein (CAPZA1:CAPZB2 heterodimer expressed in *E. coli*). Right, immunoblot analysis of purified MYC-CAPZB2 and capping protein. Detection antibodies and their targets are indicated below each immunoblot. (G) Inhibition of pyrene-actin polymerization by capping protein (left) or MYC-CAPZB2 (right). (H) Summed data. MYC-CAPZB2 data includes those with proteins purified by only 9E10 chromatography or with 9E10 and gel filtration; results were similar. Data were fit with Hill plots. For capping protein, IC50 = 2.1 ± 0.2 nM and Hill coefficient = 1.3 ± 0.2; for MYC-CAPZB2, IC50 = 190 ± 25 nM and Hill coefficient = 1.1 ± 0.1. (D–H) Transfection of utricle hair cells with MYC-CAPZB2.

control its actin binding (Edwards et al., 2014). Two of these proteins, MTPN (also known as V-1) and PLEKHO1 (also known as CKIP-1), were identified in mouse or chick hair-bundle proteome data (Table S1). Using immunocytochemistry, we were unable to detect MTPN in mouse cochlea or utricle. By contrast, an antibody against PLEKHO1 indicated that like CAPZB2, this protein is localized to bundles in a punctate pattern, with concentration toward stereocilia tips (Fig. 9, A and C). PLEKHO1 was also found along the lateral membranes of cochlear hair cells (Fig. 9 A).

PLEKHO1 immunoreactivity increased substantially in stereocilia of *Capzb*^{CKO} cochlear hair cells as compared with controls (Fig. 9, B and C). This increase was paralleled by an increase in PLEKHO1 labeling of the lateral cell body membranes of *Capzb*^{CKO} cochlear hair cells too (Fig. 9, B and C). PLEKHO1 also increased in stereocilia and lateral membranes of hair cells in *Capzb*^{CKO} utricles (Fig. 9, D and E). As with CAPZB2 (Fig. 6), PLEKHO1 immunolabeling was absent from short stereocilia of bundles from *Capzb*^{CKO} utricle hair cells (Fig. 9 E, arrow). These results suggest that CAPZB and PLEKHO1 interact functionally.

PLEKHO1 and CAPZB2 labeling partially overlapped in utricle stereocilia (Fig. 9 F). PLEKHO1 labeling appeared to be more continuous than the punctate CAPZB2 immunoreactivity, but there were clear regions of colabeling (Fig. 9 F, arrowheads in insets).

Discussion

Heterodimeric capping protein controls the length and width of stereocilia during hair-bundle development. Although capping protein is usually thought to slow polymerization of actin filaments by blocking monomer addition to barbed ends (Fig. 10 A), it also prevents depolymerization (Caldwell et al., 1989). We suggest that capping protein stabilizes actin filaments while the stereocilia core lengthens and widens, a model that is supported by three lines of evidence. First, capping protein is up-regulated in stereocilia in intermediate-sized hair bundles that are undergoing stereocilia lengthening and widening. Second, stereocilia actin is destabilized by the removal of capping protein during development of the bundle; in the *Capzb* conditional knockout, stereocilia narrowed and shortened until they largely disappeared. Finally, expression of exogenous CAPZB2 protein during early hair cell development prevented normal stereocilia elongation. These results suggest that capping protein does not simply prevent actin polymerization but instead controls access to filaments, preventing depolymerization and

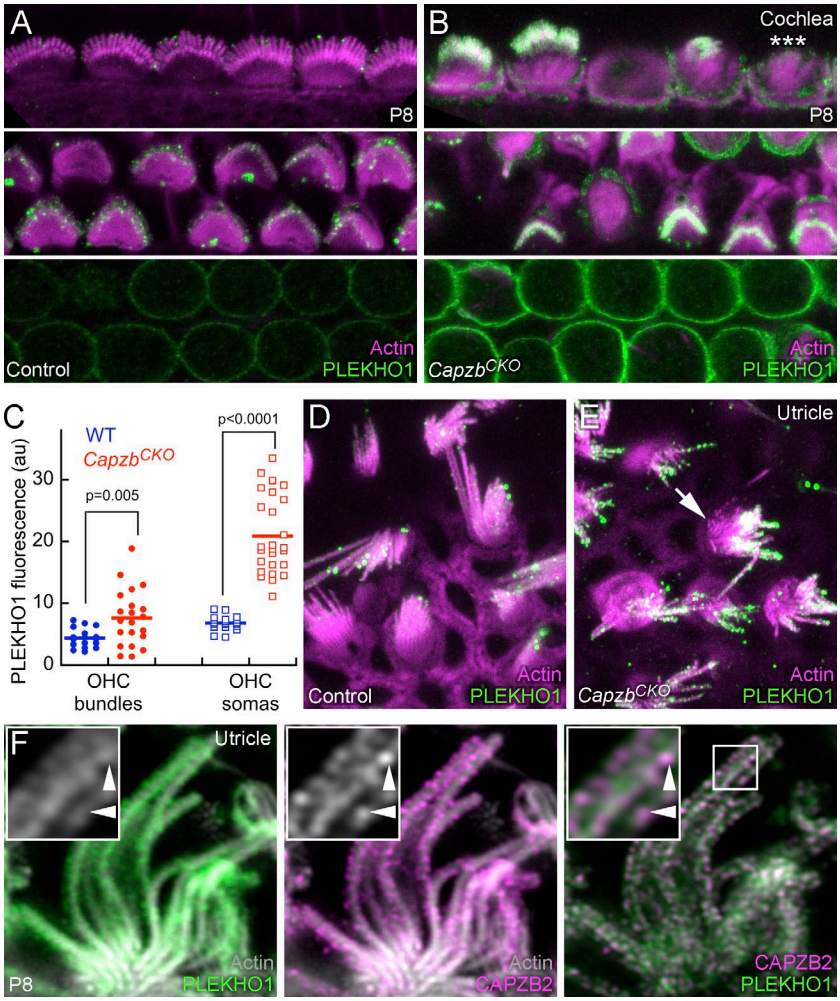

Figure 9. **PLEKHO1 is up-regulated in *Capzb*^{CKO} inner ears.** (A) Immunocytochemistry of wild-type mouse cochlea at P8 using antibody against PLEKHO1. The top panel shows inner hair cells, the middle panel shows outer hair cells, and the bottom panel shows outer hair cell somas. (B) PLEKHO1 immunoreactivity in *Capzb*^{CKO} cochlea. Asterisk indicates degenerating hair bundle with reduced PLEKHO1 immunoreactivity. (C) Quantitation of PLEKHO1 fluorescence in 2-µm z-projections using regions of interest encompassing outer hair cell (OHC) bundles or somas. (D) PLEKHO1 immunoreactivity in wild-type utricle. (E) PLEKHO1 immunoreactivity in *Capzb*^{CKO} utricle. Arrow indicates lack of staining of short stereocilia. (F) Colocalization of PLEKHO1 and CAPZB2 in P8 utricle stereocilia. Arrowheads show colocalized PLEKHO1 and CAPZB2 punctae. Panel full widths: (A and B) 50 µm; (D and E) 25 µm; (F) 12 µm (inset is 2 µm).

allowing for controlled elongation and widening at intermediate stages of bundle development. These activities are essential for hair cells, as mice lacking *Capzb* in their hair cells are profoundly deaf and have greatly diminished vestibular function.

CAPZB2 location during hair-bundle development

In the utricle, the highest concentrations of hair-bundle CAPZB2 were seen in medium-sized bundles (~5 µm) with thin stereocilia. In Tilney's description of stereocilia development (Tilney et al., 1992), stereocilia cease elongating at the end of stage 2, allowing widening in stage 3; he also suggested that actin cappers halt actin polymerization at tips, which is supported by expression analysis in chick cochlea (Avenarius et al., 2014). The medium-sized bundles we saw with high CAPZB2 presumably were undergoing stereocilia widening, consistent with Tilney's hypothesis.

Between P0 and P8, CAPZB2 was largely observed along stereocilia shafts in utricle hair cells (Fig. 10 B); immunoreactivity was sometimes seen at stereocilia tips, albeit at very low intensity. However, after P21, strong CAPZB2 labeling was clearly seen at tips of many stereocilia. The data suggest that CAPZB2 is found along stereocilia shafts during widening but that it accumulates at tips once that process has finished (Fig. 10, B and C). Collectively, the immunolocalization observations suggest that CAPZB2 helps control elongation of new actin filaments added to the sides of the preexisting actin paracrystal during the widening phase and remains at stereocilia tips to stabilize these filaments.

Misregulation of stereocilia diameter and length after loss of CAPZB

The *Capzb* knockout provided additional evidence that CAPZB controls stereocilia length and width. To circumvent embryonic lethality associated with global knockout of *Capzb*, as well as any disruption to hair cell progenitors that may also express CAPZB, we used the *Atoh1-Cre* transgenic line to restrict *Capzb* deletion to hair cells (Matei et al., 2005; Pan et al., 2012). The time course of elimination of CAPZB protein thus depended on expression kinetics for *Atoh1-Cre*, CRE recombinase activity toward both alleles of the *Capzb* gene, and decay kinetics of both CAPZB mRNA and protein. Once the *Capzb* gene has been recombined, appearance of the phenotype depends on the rate at which CAPZB disappears from hair cells and the threshold for the phenotype to manifest itself. Using immunocytochemistry, we observed that CAPZB was retained in cochlear stereocilia even when it had mostly disappeared from the hair cell soma, suggesting that CAPZB exit from stereocilia is slow. Accordingly, the phenotype varied substantially from cell to cell, even within a small cochlear area where the hair cells were of nearly the same age. The variability in phenotype was much greater in utricle, where hair cells are born over a much longer time span (Burns et al., 2012).

Loss of CAPZB in hair cells led to misregulation of length and width in stereocilia (Fig. 10 C). In both the auditory and vestibular systems, stereocilia shortened and then eventually disappeared. In the utricle, the quantitative data suggested

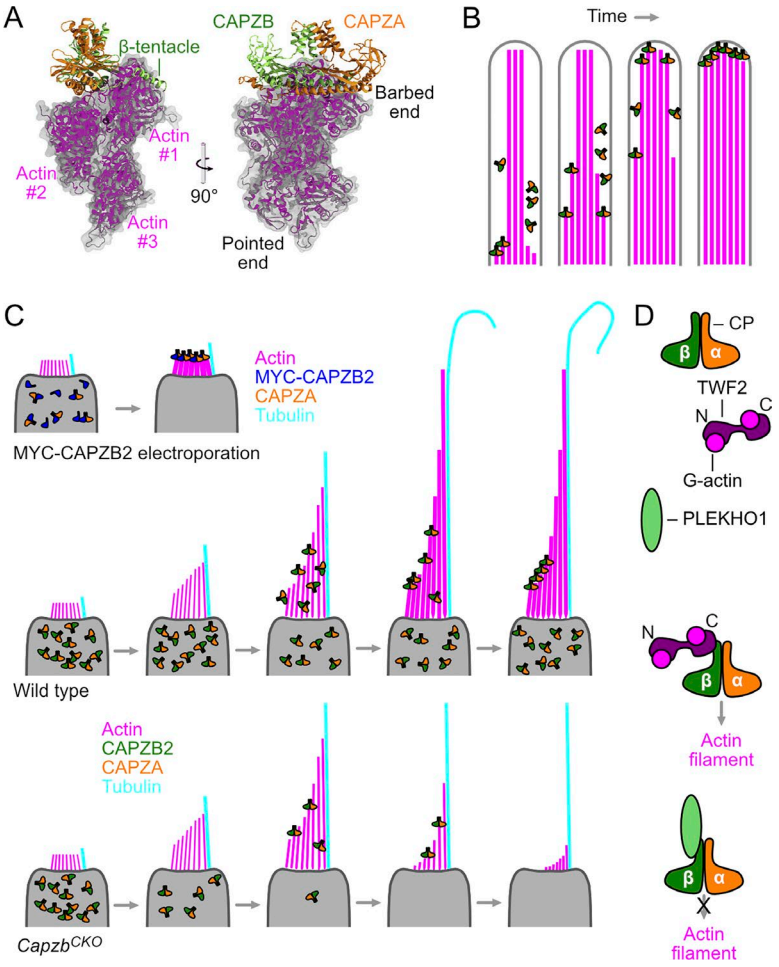

Figure 10. **CAPZB action in hair cells.** (A) Model for capping protein interaction with actin. The β-tentacle of CAPZB (dark green) wraps around the first actin subunit (of three shown; magenta). CAPZA also binds to actin with its tentacle. Panel A was modified from Kim et al. (2010) with permission. (B) Model for action of capping protein in widening; the four stereocilia cartoons indicate sequential steps in the process. New actin filaments polymerize from the stereocilia base to the tip, alongside the preexisting original actin paracrystal. Capping protein transiently binds to elongating filaments, preventing their depolymerization when actin monomers are not available. (C) Development of hair cells with or without CAPZB. The middle trajectory indicates how stereocilia lengthening and widening proceed in a wild-type hair cell, with capping protein indicated using the same color scheme as in A and B. CAPZB enters stereocilia after the initial lengthening step and is present during widening. CAPZB accumulates at stereocilia tips, at least in shorter stereocilia. The lower trajectory diagrams the narrowing and shortening of stereocilia that occurs after CAPZB is lost. CAPZB derived from hair-cell progenitors is present in *Capzb*^{CKO} even after levels drop in the soma, presumably slowing the shortening and narrowing process. The top trajectory shows the cessation of stereocilia elongation that occurs when MYC-CAPZB2 is expressed in hair cells, as well as the abnormal stereocilia widening. MYC-CAPZB2 is represented with blue subunits, both as monomers and as heterodimers with CAPZA subunits. The placement of the MYC-CAPZB2 and CAPZA molecules in the MYC-CAPZB2 scenario is based on their presumed localization. (D) Diagram of interactions between capping protein (CP), TWF2, and PLEKHO1. The N terminus of CAPZB, which is not directly involved in binding actin filaments, binds to either TWF2 (shown with bound actin monomers) or PLEKHO1.

that stereocilia grow to nearly normal dimensions, but then as CAPZB is lost, both diameter and length simultaneously decrease. The steeply graded bevels of utricle hair bundles ensured that the shorter stereocilia disappeared from the apical surface first, followed by the longer stereocilia.

The difference in phenotype between auditory and vestibular hair bundles may be caused by differences in the control of actin structures in the cells. In vestibular hair cells, the loss of actin from stereocilia was matched by a growth of actin-rich structures at the adherens junction and in cytocaud-like structures present more basally in the cell; in this case, utricular stereocilia shortened and disappeared, as actin (and other stereocilia proteins) was redirected to those soma structures. By contrast, in cochlear hair cells, actin released from shortening stereocilia apparently elongated microvilli on the apical surface; cochlear apical processes did eventually disappear, however.

MYC-CAPZB2 inhibition of stereocilia growth

Overexpression of CAPZB2 provided an additional approach for probing its role in stereocilia dimensions. When expressed in hair cells using in utero electroporation, MYC-CAPZB2 induced substantial alterations in hair-bundle structure (Fig. 10 C). Although capping protein subunits apparently do not have potent capping activity outside of the heterodimer, in both crude and purified stereocilia, there was approximately five times more CAPZA than CAPZB. By expressing MYC-CAPZB, we apparently elevated the concentration of capping protein heterodimer, which is consistent with the interference we see with stereocilia elongation and diameter control.

With transfected MYC-CAPZB2, hair bundles grew to ∼4 µm, with most stereocilia of the same length. In some cases, stereocilia diameter increased substantially; the phenotype was variable, but actin cores of some stereocilia were ∼750 nm in diameter. Presumably elevated capping protein halted stereocilia elongation and prevented formation of the staircase; that concentration of capping protein apparently did not affect stereocilia widening to the same degree, so free actin monomers could be used for increasing stereocilia diameter.

Cochlear stereocilia did not show the same short-stereocilia phenotype with MYC-CAPZB2 overexpression. As in vestibular hair cells, CAPZA1 and CAPZA2 are at much higher levels in cochlear hair cells than is CAPZB, which suggests cochlear cells could regulate assembly of heterodimers differently than do vestibular cells. Alternatively, other actin cappers may provide a stronger inhibition on stereocilia growth, so that the effects of MYC-CAPZB2 expression are minimal in cochlear hair cells.

Regulation of CAPZB

TWF2 and CAPZB2 interact in hair cells. Previous studies had shown that capping protein and twinfilin interact physically and functionally in yeast (Palmgren et al., 2001; Falck et al., 2004) and in vitro in mouse (Palmgren et al., 2001; Ewing et al., 2007; Kristensen et al., 2012). Our results show that CAPZB2 physically interacts with both TWF1 and TWF2 in the inner ear (Fig. 3)

and that CAPZB2 and TWF2 partially colocalize in stereocilia (Fig. 2 O). The physiological role of the twinfilins remains uncertain; although they have capping activity (Helfer et al., 2006; Paavilainen et al., 2007), they also bind actin monomers, a function that is essential for their activity in yeast (Palmgren et al., 2001). Although capping with one actin depolymerizing factor homology domain, twinfilins also bind to the filament's side with their second actin depolymerizing factor homology (Paavilainen et al., 2007). Plausibly a capping protein–twinfilin complex could bind to the side of a fully formed actin filament while a new filament was polymerizing, allowing regulation of capping. Because no twinfilin protein was coimmunoprecipitated with CAPZA1 or CAPZA2, however, TWF2 may not interact substantially with the heterodimer. *Twf2*-null mice do not have hearing loss (Heller, S., personal communication), but the presence of the close paralogue TWF1 may prevent loss of hair cell function. TWF2 is localized in hair bundles by MYO7A (Rzadzinska et al., 2009), suggesting that the relationships among TWF2, MYO7A, and capping protein will be important to determine.

The capping protein regulator PLEKHO1 has a very similar location to CAPZB2 in stereocilia. PLEKHO1 is known to interact with capping protein in other cell types (Canton et al., 2005), and it inhibits the actin-binding activity of capping protein (Fig. 10 D). The expression of PLEKHO1 is increased notably after *Capzb* is deleted, which suggests the level of CAPZB in hair cells directly or indirectly controls the transcription or translation of PLEKHO1. In shotgun proteomics experiments (PXD002167), we only detected PLEKHO1 in one of four P5 hair-bundle samples and not at all at P23; its apparent concentration (~71 molecules per stereocilium), however, was essentially identical to that of CAPZB (~74 molecules per stereocilium). If capping-protein heterodimer was elevated by MYC-CAPZB2 expression via in utero electroporation, the increased level could have overwhelmed control by PLEKHO1, leading to the misregulation of stereocilia growth we saw. Although gross auditory or vestibular defects were not reported for *Plekho1*-null mice (Lu et al., 2008), the paralogue *Plekho2* is expressed in the inner ear (http://gear.igs.umaryland.edu) and might compensate. Indeed, PLEKHO2 was detected in CAPZB2 immunoprecipitations (Table S3), although PLEKHO1 was not.

Role of capping protein in stereocilia growth

Controlled widening of stereocilia is an essential step in growth of a hair bundle. In mouse utricle, ESPN is required for the barbed end–directed growth of actin filaments during widening (Sekerková et al., 2011). Like with ESPN, loss of CAPZB leads to eventual stereocilia shortening, which reflects the coordination of the widening and lengthening processes. Capping protein plays a similar role in widening of filopodia, which are structurally related to stereocilia; CAPZB2 is found along the sides of filopodia shafts and may be responsible for the tapered appearance of many filopodia in B16F10 mouse melanoma cells (Sinnar et al., 2014).

In our model, capping protein is recruited during widening to prevent depolymerization of newly growing actin filaments (Fig. 10, B and C), which may be especially important if the concentration of actin monomers is limiting. As these new filaments elongate, capping protein eventually accumulates at stereocilia tips, where it helps stabilize mature stereocilia filaments. TWF2 is localized similarly along stereocilia shafts, and the CAPZB2-TWF2 interaction that occurs in stereocilia suggests that TWF2 too may regulate stereocilia widening. Like ESPN, twinfilins binds actin monomers (Goode et al., 1998), which may increase the local monomer concentration and increase polymerization of nascent filaments. In contrast, PLEKHO1 may inhibit capping protein to allow access of actin monomers to growing filament ends (Canton et al., 2006). Together, these results are consistent with a model where rather than being freely diffusible, capping protein is held in regulatory complexes that prevent unfettered actin capping and allow more control (Edwards et al., 2014).

Capping protein thus plays an essential role in formation of hair bundles. Because of the embryonic lethality associated with deletion of *Capzb* and the likely ability of the three separate genes encoding CAPZA subunits to compensate for each other, the capping protein genes are unlikely to be identified in screens for deafness mutations. Capping protein subunits were readily identified by mass spectrometry, however, affirming the value of proteomics approaches for revealing molecules underlying bundle development.

Materials and methods

Nomenclature

We refer to the α-β heterodimer of CAPZA and CAPZB subunits as "capping protein" or "heterodimeric capping protein." We use official gene symbols to refer to individual protein subunits (and other proteins), following the convention for mouse proteins (all caps and no italics). When referring specifically to the individual protein splice form, we write "CAPZB2" or "CAPZB1"; we use "CAPZB" to indicate both splice forms.

Antibodies

For CAPZB2, we used AB6017 (RRID:AB_10806205; EMD-Millipore), which has been validated as being CAPZB specific (Sinnar et al., 2014). We confirmed that similar labeling was seen in mouse utricle using an antibody raised against a mouse CAPZB2 peptide ([C]DKSKQEALKNDLVEALKRKQQS, corresponding to residues 251–272; synthesized by Genemed Synthesis). For CAPZA1, we used 11806-1-AP (RRID: AB_2070037; Proteintech); this antibody has been validated by shRNA knockdown (Lee et al., 2013). The mAb 5B12.3 (RRID: AB_531816) and mAb 3F2.3 (RRID: AB_531768) hybridoma cells (deposited by J. Cooper) and the 9E10 (RRID: AB_2266850) hybridoma cells (deposited by J.M. Bishop) were obtained from the Developmental Studies Hybridoma Bank, created by the Eunice Kennedy Shriver National Institute of Child Health and Human Development of the National Institutes of Health and maintained at the Department of Biology, University of Iowa. mAbs were produced from hybridoma cells in serum-free medium using a bioreactor and purified with protein A chromatography (VGTI Monoclonal Antibody Core; Oregon Health and Science University). The TWF2 antibody was raised against full-length mouse TWF2 and was affinity purified against the whole protein (gift of S. Heller, Stanford University, Stanford, CA); the antibody cross-reacted weakly with TWF1 as well (Fig. S1 F). Other antibodies used were EPS8 (clone 15, 610143; RRID: AB_397544; Thermo Fisher), EPS8L2 (ab57571; RRID:AB_941458; Abcam), GSN (N-18, sc-6406; RRID:AB_640946; Santa Cruz), and PLEKHO1 (clone 3D5, M01A; RRID:AB_1578891; Abnova).

Mice

Capzb$^{tm1a(EUCOMM)Wtsi}$ frozen embryos were obtained from the European Conditional Mouse Mutagenesis Program and rederived using standard

procedures; mice were backcrossed to C57BL/6 (presently eight or more generations). The FRT-flanked neo cassette was removed by crossing with the *Flp* deleter line B6;SJL-Tg(ACTFLPe)9205Dym/J (003800; Jackson Laboratories), generating *Capzb*^{fl} mice; PCR genotyping was used to verify loss of the cassette. To produce *Capzb*^{CKO} mice, we used the *Atoh1-Cre* mouse line (Matei et al., 2005), which was provided by B. Frizsch (University of Iowa, Iowa City, IA). Crossing *Atoh1-Cre* with the Ai14 reporter line (Madisen et al., 2010), we found that >99% of cochlear and vestibular hair cells, identified with anti-MYO7A, were positive for the tdTomato reporter at P2 or P7 (Fig. S3). These data coincided with previous studies demonstrating that CRE activity was widespread among hair cells using *Atoh1-Cre* (Matei et al., 2005; Pan et al., 2012). *Capzb*^{CKO} mice were then generated from a *Capzb*$^{fl/fl}$ and *Capzb*$^{+/fl}$*;Atoh1-Cre* cross; heterozygous control mice were *fl/+ Cre+*, whereas wild-type mice were *fl/fl Cre-* or *fl/+ Cre-*. We used a variety of ages for our experiments; in general, however, we used windows of P1, P7–P9, and P21–P25 for examining developmental progressions.

Expression plasmids

To generate the plasmid encoding CAPZB2 tagged with two MYC epitopes on the N terminus (MYC-CAPZB2), a double-stranded oligo encoding a start codon and the MYC tag sequence repeated twice in tandem was directionally cloned into the NheI and EcoRI sites of plasmid pMC.EF1-MCS-IRES-GFP-SV40PolyA (MN530-A1, Systems Biosciences), which coexpresses ZsGreen. Next, the open reading frame of *Capzb* (B2 splice form; NM_009798.4) was PCR amplified (forward: 5′-AATCTAGAATTCATGAGCGATCAGCAGCTGGA-3′ and reverse: 5′-TTCGTTGAATTCTCAACACTGCTGCTTTCTCTTC-3′) and cloned into the MYC-encoding pMC.EF1-MCS-IRES-GFP-SV40PolyA, which had been cut with EcoRI. Positive clones were Sanger sequenced to ensure proper insertion and nucleotide sequence of the *Capzb2* open reading frame. MYC-CAPZA1 was generated similarly. To generate N-terminal GFP tagged capping protein constructs, the open reading frame of each capping protein gene was PCR amplified (CAPZA1 forward: 5′-ATAGCACTCGAGAAATGGCCGACTTTG AGGATCG-3′ and CAPZA1 reverse: 5′-CTAGTACCGCGGTTAAGC ATTCTGCATTTCTT-3′; CAPZB1 forward: 5′-GATCTACTCG-AGC CATGAGCGATCAGCAGCTGGA-3′ and CAPZB1 reverse: 5′-CGA TTCCCGCGGTCAA-TTATCAGGCTGGATGT-3′; CAPZB2 forward: 5′-CTAGTACTCGAGAAATGAGCGATCAGCA-GCTGGA-3′ and CAPZB2 reverse: 5′-AACGTTCCGCGGTCAACACTGCTGCTT TCTCT-3′). The amplified products and the peGFP-C1 plasmid (Clontech) were digested with XhoI and SacII, purified (28704; Qiagen) and quantified. Each PCR product was independently ligated into the digested peGFP-C1 vector, and positive clones were Sanger sequenced to verify the nucleotide sequence matched the reference sequence.

Purification of MYC-CAPZB2

MYC-CAPZB2 was expressed using HEK293 cells (RRID:CVCL _0045), which were maintained in DMEM (Thermo Fisher) with glucose, pyruvate, and glutamine (D6429; Sigma-Aldrich), supplemented with 10% FBS (S11150; Atlanta Biologicals). Cells were seeded 24 h before transfection in 15-cm plates at 9×10^6 cells per well. Cells were transfected with 24 µg DNA using polyethylenimine (23966; Polysciences) and harvested 48 h later by washing the plate with PBS and centrifuging the suspension at 50 *g* (700 rpm) for 5 min. The cell pellet was diluted in PBS and centrifuged twice more before the supernatant was removed, the pellet snap frozen in liquid nitrogen, and stored at −80°C. Cells were extracted by sonication using 1% Tween-20, 150 mM NaCl, 1 mM EDTA, and 50 mM Tris, pH 8. After centrifugation at 10,000 *g* for 15 min, the supernatant was collected; the pellet was extracted a second time, and the supernatants were pooled. The combined supernatants were then centrifuged at 100,000 *g* for 30 min. The supernatant was incubated overnight with 500–750 µl 9E10 monoclonal antibody coupled to AminoLink Plus Coupling Resin (cross-linked agarose beads; 20501; Thermo Fisher); the beads were collected and washed five times with 0.01% Tween-20 in PBS. The MYC-CAPZB2 was eluted using 250 µl of 0.5 mg/ml EQKLISEEDL (RP11731-5; Genscript) in 0.01% Tween/PBS and incubating at 37°C for 15 min. The elution step was repeated at least five times. Binding and elution were repeated once, and the samples pooled. In some cases, the eluate from the 9E10 beads was concentrated and separated by gel filtration using 1× KMEI (50 mM KCl, 1 mM EGTA, 1 mM $MgCl_2$, 0.2 mM ATP, 1 mM DTT, and 10 mM imidazole, pH 7.0) and a Superdex 200 10/300 GL column.

Actin polymerization

Pyrene-labeled and unlabeled actin was obtained from B. Nolen and C. Balzer (University of Oregon, Eugene, OR) or from C. Yengo (Pennsylvania State University, State College, PA). Actin polymerization was measured in 96-well plates essentially as described previously (Rodnick-Smith et al., 2016) and was performed in 1× KMEI (50 mM KCl, 1 mM EGTA, 1 mM $MgCl_2$, 0.2 mM ATP, 0.5 mM DTT, and 10 mM imidazole, pH 7.0). In brief, to exchange Ca^{2+} for Mg^{2+}, actin (15–30% pyrene labeled) was incubated for 2 min with 2 mM EGTA and 0.5 mM $MgCl_2$. Preformed actin seeds (Kuhn and Pollard, 2007) were generated by mixing 8 µM unlabeled actin with KMEI and incubating >30 min. After vortexing for 30 s, actin seeds (final 0.3 µM) were added to all samples containing all components except G-actin. Polymerization was initiated by pipetting pyrene-actin (final 3 µM) into each sample. Fluorescence was monitored at 405 nm with excitation at 365 nm. We used bacterially expressed capping protein (CAPZA1: CAPZB2; from B. Nolen and C. Balzer) as a positive control.

Immunofluorescence and light microscopy

For labeling of *Capzb*^{CKO} utricles over development with phalloidin alone (Fig. 6, C–H), phalloidin and tdTomato (Fig. 6, A and B; Fig. 5, A and B; and Fig. 7, A–D), or primary antibodies and phalloidin (Fig. 6, I and J), as well as labeling of tissues subjected to in utero electroporation (Fig. 8, A, B, D, and E), inner ear tissue was dissected from periotic bones of mice and placed in 4% formaldehyde (1570; Electron Microscopy Sciences) for at least 1 h. The tissue was further dissected in Hank's balanced salt solution (14025076; Thermo Fisher) supplemented with 25 mM Hepes, pH 7.5 (dissection buffer). The otolithic membrane was loosened by a 20-min proteolytic digestion at room temperature in 45 µg/ml protease XXIV (P8038; Sigma-Aldrich) and was manually removed. For immunocytochemistry, tissue was washed in dissection buffer three times and permeabilized in dissection buffer supplemented with 0.2% Triton X-100, 1.0% normal donkey serum (S30-100ML; Sigma-Aldrich), and 0.1% BSA for 15 min. After another series of washes in dissection buffer, the tissue was transferred to dissection buffer supplemented with 1.0% normal donkey serum and 0.1% BSA for 1 h (blocking solution). For Figs. 6 (A and B) and 7 (A–D), organs were rinsed in PBS, permeabilized for 10 min in 0.5% Triton X-100 (for other cappers) in PBS, and blocked for 1 h in 5% normal donkey serum in PBS. The tissue was washed and incubated overnight at 4°C with primary antibody diluted in blocking solution. The next day, the tissue was washed and incubated with the secondary antibody (2 µg/ml donkey anti–mouse Alexa Fluor 647, A31571; Thermo Fisher; 2 µg/ml Alexa Fluor 555 donkey anti–rabbit IgG [H+L], A31572; Thermo Fisher) and phalloidin (Alexa Fluor 488 phalloidin; 0.4 U/ml; A12379; Thermo Fisher) diluted in blocking solution for 3 h at room temperature. For Fig. 8 (A, B, D, and E), the tissue was incubated with 2 µg/ml Alexa Fluor 488 donkey anti–mouse IgG (H+L)

(A21202; Thermo Fisher) and 0.8 U/ml CF633 phalloidin (00046; Biotium). Finally, tissue was washed three times in dissection buffer. Cochlear tissue was transferred to a microscope slide and mounted in Everbrite (23001; Biotium), whereas vestibular tissue was transferred to a microscope slide fitted with Secure-Seal spacers (S24737; Thermo Fisher) and mounted in Vectashield (H-1000; Vector Labs).

To analyze the labeling for CAPZB2 or other capping proteins over development (Fig. 2), as well as for CAPZB2, TWF2, or ESPN in *Capzb*^{CKO} mice (Fig. 5, C–F; and Fig. 6, M–P), dissected cochleae and utricles were fixed for 20 min at room temperature in 4% formaldehyde in PBS. Organs were rinsed in PBS, permeabilized for 10 min in 0.2% Triton X-100 (for CAPZB and CAPZA) or 0.5% Triton X-100 (for other cappers) in PBS and blocked for 1 h in 5% normal donkey serum in PBS. If carrying out immunocytochemistry, organs were then incubated overnight at 4°C with primary antibodies diluted in blocking solution. Tissue was then rinsed and stained with secondary antibodies (1 µg/ml donkey anti–rabbit Alexa Fluor 488; A21206; Thermo Fisher; 1 µg/ml anti-mouse Alexa Fluor 488, A21202) and Alexa Fluor 568 phalloidin (0.4 U/ml; A12380; Thermo Fisher) in the blocking solution. After washing cochleas and utricles, they were mounted using Vectashield.

For Figs. 2 O and 9 F, double labeling of the two rabbit primary antibodies was accomplished by blocking with unconjugated Fab fragments as follows. Tissue was processed as for single antibodies with an overnight incubation with the CAPZB primary antibody and a 3-h room temperature incubation with 1:1,000 donkey anti–rabbit Alexa Fluor 488 secondary antibody. After five washes in PBS, tissue was blocked for 1 h at room temperature in 10% normal rabbit serum, washed three times with PBS, and then incubated for 2 h in 50 µg/ml donkey anti–rabbit Fab fragments (711-007-003; Jackson ImmunoResearch). Tissue was rinsed three times in PBS and then incubated overnight at 4°C with the second rabbit primary antibody, washed three times in PBS, and then incubated for 3–4 h at room temperature in 1 µg/ml donkey anti–rabbit Alexa Fluor 568 secondary antibodies (A10042; Thermo Fisher) and 0.8 U/ml CF405M phalloidin (00034; Biotium). Tissue was washed and then mounted in Vectashield.

Isolated stereocilia samples were prepared as described previously (Krey et al., 2016), with the following differences. Square #1.5 glass coverslips were soaked with a 4% ammonium hydroxide and 4% hydrogen peroxide solution, washed with multiple changes of water, and soaked in methanol. Before use, methanol was mostly removed by air drying, and then the coverslip was briefly passed through a flame and allowed to dry completely. Coverslips were then coated with 100 µg/ml poly-lysine for 10–20 min and then dried for 30–60 min. Dissected utricles were dropped onto the coverslips in dissection media and gently pressed to the coverslip with the epithelium side down. The utricle and dissection solution was then removed, and 200 µl of 4% formaldehyde in PBS was added to each coverslip for 20 min. Samples were permeabilized for 10 min in 0.1% Triton X-100, incubated overnight with Alexa Fluor 488 phalloidin, washed with PBS, and then mounted with Vectashield. For analysis of CAPZB2 signal, coverslips were permeabilized for 10 min in 0.1% Triton X-100, blocked for 1 h with 5% normal donkey serum, and incubated overnight at 4°C with CAPZB2 primary antibodies. Coverslips were then gently washed with PBS, incubated with donkey anti–rabbit Alexa Fluor 568 and Alexa Fluor 488 phalloidin for 3 h, rinsed, and then mounted with Vectashield. We measured length using maximum projections. To measure diameter, we fit a transect of an average projection of a stereocilium with a single Gaussian and then took the full width at half-maximum (FWHM) as an estimate for the diameter. The point-spread function for the microscope using the same imaging conditions (Fig. S1, E and F) indicated that diffraction adds <200 nm to the estimate of diameter.

We performed image-scanning microscopy (Müller and Enderlein, 2010; Sheppard et al., 2013; Roth et al., 2016) using a 63×, 1.4 NA Plan-Apochromat objective or 25× 0.8 NA Plan-Neofluar (Fig. 6, A and B) on a Zeiss Elyra PS.1, equipped with an Airyscan detector; images were processed using ZEN 2012 (black edition, 64-bit software; Zeiss) version 8.0 with default settings. For conventional confocal microscopy, samples were imaged with an integrated photomultiplier tube on either an LSM 710 (Zeiss) fitted with 63×, 1.4 NA Plan-Apochromat objective or 25× 0.8 NA Plan-Neofluar objectives or on an Olympus FluoView 1000 using a 60×, 1.42 NA Plan-Apochromat objective. All microscopy was performed at room temperature.

For images acquired as z-stacks using conventional confocal microscopy, we used Reslice in Fiji/ImageJ to get a cross section. For the low-magnification images of Fig. 2 (A–L), we took 10-µm-deep x-z reslices and then maximum projected the reslices. Some Airyscan images were analyzed in a similar manner, but to acquire the high-magnification images for Fig. 2 (A–L), we found regions where hair bundles were visible in profile in a single section and then acquired the z-stack through the bundles. We then average-projected three to five z-slices to obtain the displayed images.

To analyze the CAPZB2 signal over development, z-series were obtained for each developmental age using the same microscope settings. Average projections, 14 µm in z, were made so that the bundle from cuticular plate to tip was included, but not the cytoplasm. Only bundles with their bases at the same z-level were quantified for a single projection; multiple projections from the same z-stack allowed us to measure all the bundles in a stack. Regions of interest were defined in Fiji using the phalloidin channel and measurements were made of the phalloidin and anti-CAPZB2 channels. Adjacent areas lacking signal were used to adjust for background fluorescence. The mean signal in each channel corresponds to the labeling density averaged throughout the bundle; the CAPZB2/phalloidin ratio represents the density of CAPZB2 relative to phalloidin in that bundle. Bundle heights were measured by comparing the z-height of the cuticular plate and the z-height of tallest stereocilia, taking into account the z-interval (0.35 µm).

Airyscan z-stacks of CAPZB2 mutants were analyzed using Fiji and Bitplane Imaris 8. Kinocilia and stereocilia length measurements were made using "Filaments" tool under manual mode in Imaris. The lower and upper end of the longest stereocilium within each bundle was manually marked with a point within the 3D projection and then a filament connecting these points was automatically drawn and measured. Bundle area, stereocilia width, and stereocilia number measurements were made in Fiji using the line and counter measurement functions. Bundle bevel measurements were made in Fiji by counting the number of stereocilia in the bundle at z-section intervals (0.925 µm), starting at the height of the cuticular plate and ending at the height of tallest stereocilia.

For point spread function (PSF) measurements, TetraSpeck microspheres of 100 nm diameter (T7279; Thermo Fisher) were air-dried onto a poly-lysine–coated, high-performance coverslip (474030-9000-000; Zeiss), and then mounted on a slide with Vectashield. A z-stack was acquired around the center of the bead using the optimal step size suggested by the ZEN 2012 software. Channel-specific point-spread functions averaged over autodetected features in the image stack were calculated using the experimental PSF dialog in ZEN 2012 using default parameters.

Scanning electron microscopy

Mice were euthanized by cervical dislocation and periotic bones were submerged in 4% formaldehyde; openings to the inner ear were made to allow penetration of the fixative. After overnight incubation at 4°C, the tissue was transferred to scanning electron microscopy

dissection buffer (50 mM Hepes, pH 7.5, 2 mM $CaCl_2$, 1 mM $MgCl_2$, and 150 mM NaCl), and further dissection was performed to isolate the cochlear and vestibular sensory epithelium. For cochlear tissue, the tectorial membrane was manually removed without protease digestion, whereas the utricle was incubated in 45 µg/ml protease XXIV (P8038; Sigma-Aldrich) for 20 min to aid in removal of the otoconia. The tissue was further fixed in 2.5% glutaraldehyde and 150 mM cacodylate buffer at pH 7.4 and incubated overnight. The tissue was processed for electron microscopy by the osmium-thiocarbohydrazide method. In brief, the tissue was incubated for 1 h in 1% (wt/vol) OsO_4, extensively washed in water, and incubated in 1% thiocarbohydrazide for 20 min. This sequence was repeated a total of three times. Next, the tissue was dehydrated with graded ethanol washes and critical-point dried using liquid CO_2. Samples were immobilized on stubs using colloidal silver and imaged using a FEI Sirion XL30 FEG scanning electron microscope or a FEI Helios Nanolab 660 DualBeam Microscope.

Shotgun mass spectrometry reanalysis

We analyzed three E20 chick and two P23 mouse mass spectrometry datasets (Table S1), each of which contains both hair bundles and whole utricle or utricular epithelium. Chick and mouse utricles at these ages have mostly mature hair cells. The original version of one dataset was described previously (Shin et al., 2013) and was reanalyzed for this manuscript (ProteomeXchange PXD002445); technical validation of the remaining three datasets has been described elsewhere (Krey et al., 2015; Wilmarth et al., 2015). This validation includes calculation of the associated false discovery rates, which were determined using a reversed-entry decoy database. These datasets are available from ProteomeXchange (Vizcaíno et al., 2014) with the accession numbers PXD002167, PXD002410, and PXD002414.

Proteins in all five datasets were annotated with protein symbols that correspond to human gene symbols. In some cases, this required referring to a mouse protein with its human symbol (e.g., DFNB31 instead of WHRN). Chicken proteins in particular required manual assessment of the appropriate symbol, as available databases (e.g., BioMart) are incomplete. We then prepared separate lists of protein symbols for chick and mouse. In each individual dataset, multiple protein groups have several protein symbols associated with them; if at least one symbol was shared between protein groups in two datasets, all symbols were combined. x_k and error values from all entries in a single protein group were combined together and reported in Table S1. Further manipulation of those data (calculation of bundle-to-epithelium ratio for each dataset and averaging of results from all three chick datasets) was performed in Table S1. The final false discovery rate for the merged chicken dataset was only 0.1%.

Quantitation in these datasets used relative intensity–based absolute quantification (riBAQ) using MS1 intensities or normalized molar intensity (i_m) using MS2 intensities; both methods are accurate, but exhibit significant protein-to-protein variation (Krey et al., 2014). We assumed that for each protein, riBAQ or i_m is identical to the protein's relative molar fraction (x_k) in the sample. Given an accurate concentration for one hair-bundle protein, concentrations for all other proteins can be estimated. We previously determined that chick utricle hair bundles contain on average ∼400,000 actin molecules (Shin et al., 2013). Although dimensions of mouse and rat utricle bundles are somewhat different, to enable comparison of abundance between datasets, we assumed 400,000 actin molecules per stereocilium in mouse and rat bundles as well. To calculate the estimated molecules per stereocilium, we used the following equation:

$$\text{Molecules per stereocilium} = \frac{x_k(molecules)}{x_k(actin)} \times 400,000.$$

Immunoprecipitation from enriched mouse stereocilia

By capturing stereocilia with wheat-germ agglutinin instead of anti-PTPRQ, we adapted our previously described method for enrichment of stereocilia membranes (Morgan et al., 2016) to mouse inner ear. Adult mouse periotic bones were dissected and frozen at −80°C before use. Using a Powergen 125 homogenizer, 200 periotic bones were disrupted in SPN buffer (S; 155 mM NaCl, 6 mM KCl, 2 mM $MgCl_2$, 4 mM $CaCl_2$, 3 mM D-glucose, and 10 mM Hepes, pH 7.25), with 1:100 Protease Inhibitor Cocktail (P; P8340; Sigma-Aldrich) and 2% normal donkey serum (N; Jackson ImmunoResearch). The suspension was then homogenized with 20 strokes in a Teflon-glass Dounce homogenizer. The sample was spun at 120 *g*, yielding 50 ml postnuclear supernatant. The postnuclear supernatant was divided and spun onto six 1-ml 75% sucrose cushions at 8,400 *g*. The cushion material was diluted with SPN and was respun onto four 1-ml 75% sucrose cushions. The pellet was homogenized with a Dounce to dissipate the crude hair bundles in 28 ml SPN.

As the D10 antibody used previously (Morgan et al., 2016) does not bind to mouse PTPRQ, we instead enriched stereocilia using WGA. WGA was conjugated at 12.5 mg protein per milliliter of beads to 1 µm MyOne Tosylactivated Dynabeads (65502; Life Technologies) as described previously (Morgan et al., 2016). The suspended crude hair bundles were rotated overnight with 0.5 ml WGA-tosyl beads. The beads were collected with a magnet, and the procedure was repeated with a second aliquot of beads. The beads were pooled and washed with SPN and then washed with SP (SPN without serum). Bound stereocilia membranes were sonicated off and washed with SP.

The crude membrane pellet was solubilized in 5 ml of RIPA buffer (50 mM Tris, pH 8.0, 150 mM NaCl, 0.1% SDS, 1% NP-40, 0.5% deoxycholate, and 1:100 protease inhibitors). Aliquots were saved at this point for analysis of immunoprecipitation starting material (total). For each immunoprecipitation, we incubated 1,875 µl (75 ear-equivalents) of the RIPA extract with 20 µl of magnetic beads conjugated with 2 mg control IgG antibody per millimeter of bead. After rotating 1 h at room temperature, control beads were collected with a magnet, washed five times with RIPA buffer, and eluted five times with 20 µl 2% SDS. To the control flow-through solution, anti-CAPZ beads were added; the incubation, washing, and elution were performed identically.

Shotgun mass spectrometry was performed as described previously (Morgan et al., 2016). Briefly, samples were prepared using the enhanced filter-aided sample preparation method (Erde et al., 2014) and analyzed with an Orbitrap Fusion Tribrid mass spectrometer (Thermo Fisher) coupled to a Thermo/Dionex Ultimate 3000 Rapid Separation UPLC system and EasySpray nanosource. MaxQuant (Cox and Mann, 2008) and the search engine Andromeda (Cox et al., 2011) were used to identify peptides and assemble proteins from the mass spectrometer RAW files. MaxQuant was used to calculate iBAQ (Schwanhäusser et al., 2011) for each protein, which we used to estimate riBAQ (Shin et al., 2013; Krey et al., 2014) and enrichment values. Mass spectrometry data, as well as spreadsheets with all derived values, are available from ProteomeXchange using the accession no. PXD006077; information conforming to Minimal Information About a Proteomics Experiment standards (Taylor et al., 2007) is included in the submission.

Mass spectrometry on FACS-sorted cochlea and utricle cells

Cells were isolated from P0, P4, or P7 cochleas and utricles of *Pou4f3-8.5-Gfp* mice (Masuda et al., 2011) using FACS. Utricles and cochleae were dissected in <1 h in PBS and then collected in DMEM (Life Technologies) with 5% FBS on ice. Utricles were dissected from the temporal bone; at postnatal stages, they were incubated for 2 min in 0.1 mg/ml protease XXIV (Sigma-Aldrich) to remove the otoconia. Cochleae were dissected and freed from the spiral ganglion and Reissner's membrane,

exposing the sensory epithelium. Organs were incubated at 37°C in 1 mg/ml dispase (Gibco) and 1 mg/ml collagenase I (Worthington) to dissociate cells; 100 µl was used for 10–12 utricles, whereas 200 µl was used for 10–12 cochleae. Protease digestion was performed for 30 min at P0 or 45 min at P4 and P7; cells were dissociated by triturating with a pipette while observing with an inverted microscope. Dissociation buffer (#13151-014; Gibco) with 5% FBS was added to complete the dissociation, tissues were filtered through a 40 µm cell strainer, and cells were sorted on a BD FACS Aria II cell sorter using a 100 µm nozzle and low pressure. The cells with the brightest signal in the GFP channel were sorted into the GFP+ pool and the cells with the lowest signal in the GFP channel were sorted into the GFP− pools, which were frozen in PBS as individual aliquots. Individual sorting runs generated from 100 to 15,000 cells, which were frozen as individual aliquots. Samples of whole cochlea or whole utricle were also isolated. We analyzed proteins from triplicate pools of 5,000 GFP-positive or GFP-negative cells from each of three developmental time points. After pooling samples, they were processed for mass spectrometry using enhanced filter-aided sample preparation (Erde et al., 2014). Samples were then subjected to liquid-chromatography mass spectrometry using DDA or DIA settings. For comparison of the same protein across multiple samples, DIA has accuracy and precision that is closer to that of targeted proteomics methods, although comparison between proteins is less accurate (Gillet et al., 2012).

For DDA, protein digests were separated using liquid chromatography with a NanoAcquity UPLC system (Waters) and then delivered to a Q Exactive HF (Thermo Fisher) using electrospray ionization with a Nano Flex Ion Spray Source (Thermo Fisher) fitted with a 20-µm stainless steel nano-bore emitter spray tip and 1.0-kV source voltage. Xcalibur version 4.0 was used to control the system. Samples were applied at 15 µl/min to a Symmetry C18 trap cartridge (Waters) for 10 min and then switched onto a 75 µm × 250 mm NanoAcquity BEH 130 C18 column with 1.7 µm particles (Waters) using mobile phases water (A) and acetonitrile (B) containing 0.1% formic acid, 7.5–30% acetonitrile gradient over 60 min, and a 300 nl/min flow rate. Survey mass spectra were acquired over m/z 395–1,005 at 120,000 resolution (at 200 m/z) and DDA selected the top 10 most abundant precursor ions for tandem mass spectrometry (MS/MS) by higher-energy collisional dissociation fragmentation using an isolation width of 1.2 m/z, normalized collision energy of 26, and a resolution of 30,000. Dynamic exclusion was set to auto, charge state for MS/MS +2 to +7, maximum ion time 100 ms, and minimum automatic gain control target of 3×10^6 in MS1 mode and 5×10^3 in MS2 mode.

For DIA, protein digests were separated using liquid chromatography and ionization as described for DDA. The DIA method was constructed using 20 m/z quadrupole isolation windows; a full scan at 30,000 FWHM resolving power (at 200 m/z) was performed followed by sequential higher-energy collisional dissociation MS/MS scans at normalized collision energy of 26 and 15,000 FWHM resolution. The range between 395 and 1005 m/z was surveyed by these experiments with maximum injection times of 55 ms and auto for MS and MS/MS, respectively. Automatic gain control values were set to 3×10^6 for MS and 10^6 for MS/MS. MS/MS scan range was set to 200–2,000 m/z.

DDA data were searched with Andromeda (Cox et al., 2011) and analyzed using MaxQuant (Cox and Mann, 2008), using peptide and protein false discovery rates of 1%; these data were used for generating the spectral library. DIA data were analyzed with Skyline (MacLean et al., 2010; Egertson et al., 2015). Skyline does not calculate false discovery rates for DIA identifications, but the spectral library is made up only of peptides identified with a false discovery rate of 1%. Mass spectrometry data, as well as spreadsheets with all derived values, are available from ProteomeXchange using PXD006240. DIA data were analyzed using DDA-derived spectral libraries and Skyline (MacLean et al., 2010; Egertson et al., 2015).

Statistical methods

The Student's *t* test was used for all pairwise comparisons (two-sided, two-sample equal variance). Data distribution was assumed to be normal but this was not formally tested.

Other methods

ABRs, DPOAEs, and VsEPs were performed as described previously (Krey et al., 2016). For these experiments, we used 12 wild-type mice (3.8 ± 0.1 mo old), nine heterozygous mice (3.9 ± 0.1 mo old), and five $Capzb^{CKO}$ mice (3.8 ± 0.2 mo old). In utero gene delivery using electroporation was performed as described previously (Ebrahim et al., 2016); for cochlea cells, GFP was detected with an antibody or the MYC epitope using 9E10 and donkey anti–mouse Alexa Fluor 647. For detection of transfected cells in the utricle, we used 9E10 immunocytochemistry with donkey anti–mouse Alexa Fluor 488; the MYC and ZsGreen signals thus overlapped, which increased our ability to detect transfected cells.

Online supplemental material

Fig. S1 shows a peptide blocking control for the CAPZB2 antibody, measurement of the PSF for image-scanning microscopy, and cross-reactivity of the anti-TWF2 antibody to TWF1. Fig. S2 shows immunoprecipitation of chicken capping protein subunits from crude chick stereocilia extracts, alignment of mouse PDK1 and PDK3 to the capping-protein interaction consensus sequence, and coimmunoprecipitation of CAPZA and CAPZB with an antibody against the DLAT subunit of the PDH complex. Fig. S3 shows >99% recombination of floxed tdTomato in vestibular and cochlear hair cells by *Atoh1-Cre*. Fig. S4 shows the $Capzb^{CKO}$ phenotype in P1 apical and basal cochlear hair cells and CAPZB2 immunoreactivity in P4 cochlea. Fig. S5 shows in utero electroporation of GFP-CAPZB2, MYC-CAPZB2, and MYC-CAPZA1 in cochlear hair cells, as well as injectoporation of GFP-CAPZA1 and GFP-CAPZB1 in cochlear hair cells. Table S1 shows DDA mass spectrometry results for isolated hair bundles and whole utricles from chick and mouse utricles. Table S2 shows mass spectrometry results from DDA and DIA analysis of FACS-sorted utricle and cochlea cells. Table S3 shows mass spectrometry results for the CAPZA1/2 and CAPZB2 immunoprecipitation experiments. Video 1 shows the behavioral phenotype of $Capzb^{CKO}$ mice.

Acknowledgments

We thank Ruby Larisch for mouse husbandry, Michael Bateschell for in utero electroporation, Ashok Reddy for assistance in developing DIA methods, Brad Nolen and Connor Balzer for pyrene-labeled actin and mouse capping protein, Chris Yengo for pyrene-labeled actin, Stefan Heller for the anti-TWF2 antibody, Bernd Fritzsch for the *Atoh1-Cre* mouse line, and John Cooper for helpful discussions and comments on the manuscript. The $Capzb^{tm1a(EUCOMM)Wtsi}$ mouse line, generated by the European Conditional Mouse Mutagenesis Program, was obtained from the European Mouse Mutant Archive.

We received support from the following core facilities: mass spectrometry from the University of Virginia W.M. Keck Biomedical Mass Spectrometry Lab and the Oregon Health and Science University (OHSU) Proteomics Shared Resource (partial support from National Institutes of Health core grants P30 EY010572 and P30 CA069533; Orbitrap Fusion S10 OD012246), mouse rederivation from the OHSU Transgenic Mouse Models core, monoclonal antibody purification from the Vaccine and Gene Therapy Institute Monoclonal Antibody Core (OHSU), confocal microscopy from the OHSU

Advanced Light Microscopy Core at The Jungers Center (P30 NS061800 provided support for imaging), and electron microscopy from the Center for Electron Microscopy and Nanofabrication at Portland State University and the OHSU Multiscale Microscopy Core. Technical support was provided by the OHSU-FEI Living Lab and the OHSU Center for Spatial Systems Biomedicine. P.G. Barr-Gillespie was supported by National Institutes of Health grants R01 DC002368, R01 DC011034, and P30 DC005983; P.G. Barr-Gillespie and U. Müller were supported by a National Institutes of Health multi-PI grant (R01 DC014427). D.P. Corey was supported by National Institutes of Health grant R01 DC002281.

The authors declare no competing financial interests.

Submitted: 30 April 2017
Revised: 21 July 2017
Accepted: 8 August 2017

References

Agrawal, A., and D.G. Schatz. 1997. RAG1 and RAG2 form a stable postcleavage synaptic complex with DNA containing signal ends in V(D)J recombination. *Cell.* 89:43–53. http://dx.doi.org/10.1016/S0092-8674(00)80181-6

Amatruda, J.F., D.J. Gattermeir, T.S. Karpova, and J.A. Cooper. 1992. Effects of null mutations and overexpression of capping protein on morphogenesis, actin distribution and polarized secretion in yeast. *J. Cell Biol.* 119:1151–1162. http://dx.doi.org/10.1083/jcb.119.5.1151

Avenarius, M.R., K.W. Saylor, M.R. Lundeberg, P.A. Wilmarth, J.B. Shin, K.J. Spinelli, J.M. Pagana, L. Andrade, B. Kachar, D. Choi, et al. 2014. Correlation of actin crosslinker and capper expression levels with stereocilia growth phases. *Mol. Cell. Proteomics.* 13:606–620. http://dx.doi.org/10.1074/mcp.M113.033704

Barr-Gillespie, P.G. 2015. Assembly of hair bundles, an amazing problem for cell biology. *Mol. Biol. Cell.* 26:2727–2732. http://dx.doi.org/10.1091/mbc.E14-04-0940

Bucks, S.A., B.C. Cox, B.A. Vlosich, J.P. Manning, T.B. Nguyen, and J.S. Stone. 2017. Supporting cells remove and replace sensory receptor hair cells in a balance organ of adult mice. *eLife.* 6:e18128. http://dx.doi.org/10.7554/eLife.18128

Burns, J.C., D. On, W. Baker, M.S. Collado, and J.T. Corwin. 2012. Over half the hair cells in the mouse utricle first appear after birth, with significant numbers originating from early postnatal mitotic production in peripheral and striolar growth zones. *J. Assoc. Res. Otolaryngol.* 13:609–627. http://dx.doi.org/10.1007/s10162-012-0337-0

Caldwell, J.E., S.G. Heiss, V. Mermall, and J.A. Cooper. 1989. Effects of CapZ, an actin capping protein of muscle, on the polymerization of actin. *Biochemistry.* 28:8506–8514. http://dx.doi.org/10.1021/bi00447a036

Canton, D.A., M.E. Olsten, K. Kim, A. Doherty-Kirby, G. Lajoie, J.A. Cooper, and D.W. Litchfield. 2005. The pleckstrin homology domain-containing protein CKIP-1 is involved in regulation of cell morphology and the actin cytoskeleton and interaction with actin capping protein. *Mol. Cell. Biol.* 25:3519–3534. http://dx.doi.org/10.1128/MCB.25.9.3519-3534.2005

Canton, D.A., M.E. Olsten, H. Niederstrasser, J.A. Cooper, and D.W. Litchfield. 2006. The role of CKIP-1 in cell morphology depends on its interaction with actin-capping protein. *J. Biol. Chem.* 281:36347–36359. http://dx.doi.org/10.1074/jbc.M607595200

Chhabra, E.S., and H.N. Higgs. 2007. The many faces of actin: Matching assembly factors with cellular structures. *Nat. Cell Biol.* 9:1110–1121. http://dx.doi.org/10.1038/ncb1007-1110

Cox, J., and M. Mann. 2008. MaxQuant enables high peptide identification rates, individualized p.p.b.-range mass accuracies and proteome-wide protein quantification. *Nat. Biotechnol.* 26:1367–1372. http://dx.doi.org/10.1038/nbt.1511

Cox, J., N. Neuhauser, A. Michalski, R.A. Scheltema, J.V. Olsen, and M. Mann. 2011. Andromeda: A peptide search engine integrated into the MaxQuant environment. *J. Proteome Res.* 10:1794–1805. http://dx.doi.org/10.1021/pr101065j

Denman-Johnson, K., and A. Forge. 1999. Establishment of hair bundle polarity and orientation in the developing vestibular system of the mouse. *J. Neurocytol.* 28:821–835. http://dx.doi.org/10.1023/A:1007061819934

Ebrahim, S., M.R. Avenarius, M. Grati, J.F. Krey, A.M. Windsor, A.D. Sousa, A. Ballesteros, R. Cui, B.A. Millis, F.T. Salles, et al. 2016. Stereocilia-staircase spacing is influenced by myosin III motors and their cargos espin-1 and espin-like. *Nat. Commun.* 7:10833. http://dx.doi.org/10.1038/ncomms10833

Edwards, M., A. Zwolak, D.A. Schafer, D. Sept, R. Dominguez, and J.A. Cooper. 2014. Capping protein regulators fine-tune actin assembly dynamics. *Nat. Rev. Mol. Cell Biol.* 15:677–689. http://dx.doi.org/10.1038/nrm3869

Egertson, J.D., B. MacLean, R. Johnson, Y. Xuan, and M.J. MacCoss. 2015. Multiplexed peptide analysis using data-independent acquisition and Skyline. *Nat. Protoc.* 10:887–903. http://dx.doi.org/10.1038/nprot.2015.055

Erde, J., R.R. Loo, and J.A. Loo. 2014. Enhanced FASP (eFASP) to increase proteome coverage and sample recovery for quantitative proteomic experiments. *J. Proteome Res.* 13:1885–1895. http://dx.doi.org/10.1021/pr4010019

Ewing, R.M., P. Chu, F. Elisma, H. Li, P. Taylor, S. Climie, L. McBroom-Cerajewski, M.D. Robinson, L. O'Connor, M. Li, et al. 2007. Large-scale mapping of human protein-protein interactions by mass spectrometry. *Mol. Syst. Biol.* 3:89. http://dx.doi.org/10.1038/msb4100134

Falck, S., V.O. Paavilainen, M.A. Wear, J.G. Grossmann, J.A. Cooper, and P. Lappalainen. 2004. Biological role and structural mechanism of twinfilin-capping protein interaction. *EMBO J.* 23:3010–3019. http://dx.doi.org/10.1038/sj.emboj.7600310

Furness, D.N., S.L. Johnson, U. Manor, L. Rüttiger, A. Tocchetti, N. Offenhauser, J. Olt, R.J. Goodyear, S. Vijayakumar, Y. Dai, et al. 2013. Progressive hearing loss and gradual deterioration of sensory hair bundles in the ears of mice lacking the actin-binding protein Eps8L2. *Proc. Natl. Acad. Sci. USA.* 110:13898–13903. http://dx.doi.org/10.1073/pnas.1304644110

Geisberg, J.V., and K. Struhl. 2004. Quantitative sequential chromatin immunoprecipitation, a method for analyzing co-occupancy of proteins at genomic regions in vivo. *Nucleic Acids Res.* 32:e151. http://dx.doi.org/10.1093/nar/gnh148

Géléoc, G.S., J.R. Risner, and J.R. Holt. 2004. Developmental acquisition of voltage-dependent conductances and sensory signaling in hair cells of the embryonic mouse inner ear. *J. Neurosci.* 24:11148–11159. http://dx.doi.org/10.1523/JNEUROSCI.2662-04.2004

Gillet, L.C., P. Navarro, S. Tate, H. Rost, N. Selevsek, L. Reiter, R. Bonner, and R. Aebersold. 2012. Targeted data extraction of the MS/MS spectra generated by data-independent acquisition: A new concept for consistent and accurate proteome analysis. *Mol. Cell. Proteomics.* 11:O111.016717. http://dx.doi.org/10.1074/mcp.O111.016717

Goode, B.L., D.G. Drubin, and P. Lappalainen. 1998. Regulation of the cortical actin cytoskeleton in budding yeast by twinfilin, a ubiquitous actin monomer-sequestering protein. *J. Cell Biol.* 142:723–733. http://dx.doi.org/10.1083/jcb.142.3.723

Helfer, E., E.M. Nevalainen, P. Naumanen, S. Romero, D. Didry, D. Pantaloni, P. Lappalainen, and M.F. Carlier. 2006. Mammalian twinfilin sequesters ADP-G-actin and caps filament barbed ends: Implications in motility. *EMBO J.* 25:1184–1195. http://dx.doi.org/10.1038/sj.emboj.7601019

Hertzog, M., F. Milanesi, L. Hazelwood, A. Disanza, H. Liu, E. Perlade, M.G. Malabarba, S. Pasqualato, A. Maiolica, S. Confalonieri, et al. 2010. Molecular basis for the dual function of Eps8 on actin dynamics: Bundling and capping. *PLoS Biol.* 8:e1000387. http://dx.doi.org/10.1371/journal.pbio.1000387

Hickox, A.E., A.C. Wong, K. Pak, C. Strojny, M. Ramirez, J.R. Yates III, A.F. Ryan, and J.N. Savas. 2017. Global analysis of protein expression of inner ear hair cells. *J. Neurosci.* 37:1320–1339. http://dx.doi.org/10.1523/JNEUROSCI.2267-16.2016

Jo, Y.J., W.I. Jang, S. Namgoong, and N.H. Kim. 2015. Actin-capping proteins play essential roles in the asymmetric division of maturing mouse oocytes. *J. Cell Sci.* 128:160–170. http://dx.doi.org/10.1242/jcs.163576

Kaltenbach, J.A., P.R. Falzarano, and T.H. Simpson. 1994. Postnatal development of the hamster cochlea. II. Growth and differentiation of stereocilia bundles. *J. Comp. Neurol.* 350:187–198. http://dx.doi.org/10.1002/cne.903500204

Kanzaki, S., L.A. Beyer, B. Canlon, W.M. Meixner, and Y. Raphael. 2002. The cytocaud: A hair cell pathology in the waltzing Guinea pig. *Audiol. Neurootol.* 7:289–297. http://dx.doi.org/10.1159/000064447

Kim, T., J.A. Cooper, and D. Sept. 2010. The interaction of capping protein with the barbed end of the actin filament. *J. Mol. Biol.* 404:794–802. http://dx.doi.org/10.1016/j.jmb.2010.10.017

Krey, J.F., P.A. Wilmarth, J.B. Shin, J. Klimek, N.E. Sherman, E.D. Jeffery, D. Choi, L.L. David, and P.G. Barr-Gillespie. 2014. Accurate label-free protein quantitation with high- and low-resolution mass spectrometers. *J. Proteome Res.* 13:1034–1044. http://dx.doi.org/10.1021/pr401017h

Krey, J.F., N.E. Sherman, E.D. Jeffery, D. Choi, and P.G. Barr-Gillespie. 2015. The proteome of mouse vestibular hair bundles over development. *Sci. Data.* 2:150047. http://dx.doi.org/10.1038/sdata.2015.47

Krey, J.F., E.S. Krystofiak, R.A. Dumont, S. Vijayakumar, D. Choi, F. Rivero, B. Kachar, S.M. Jones, and P.G. Barr-Gillespie. 2016. Plastin 1 widens

stereocilia by transforming actin filament packing from hexagonal to liquid. *J. Cell Biol.* 215:467–482. http://dx.doi.org/10.1083/jcb.201606036

Kristensen, A.R., J. Gsponer, and L.J. Foster. 2012. A high-throughput approach for measuring temporal changes in the interactome. *Nat. Methods.* 9:907–909. http://dx.doi.org/10.1038/nmeth.2131

Kuhn, J.R., and T.D. Pollard. 2007. Single molecule kinetic analysis of actin filament capping. Polyphosphoinositides do not dissociate capping proteins. *J. Biol. Chem.* 282:28014–28024. http://dx.doi.org/10.1074/jbc.M705287200

Lee, Y.J., S.H. Jeong, S.C. Hong, B.I. Cho, W.S. Ha, S.T. Park, S.K. Choi, E.J. Jung, Y.T. Ju, C.Y. Jeong, et al. 2013. Prognostic value of CAPZA1 overexpression in gastric cancer. *Int. J. Oncol.* 42:1569–1577. http://dx.doi.org/10.3892/ijo.2013.1867

Lu, K., X. Yin, T. Weng, S. Xi, L. Li, G. Xing, X. Cheng, X. Yang, L. Zhang, and F. He. 2008. Targeting WW domains linker of HECT-type ubiquitin ligase Smurf1 for activation by CKIP-1. *Nat. Cell Biol.* 10:994–1002. http://dx.doi.org/10.1038/ncb1760

MacLean, B., D.M. Tomazela, N. Shulman, M. Chambers, G.L. Finney, B. Frewen, R. Kern, D.L. Tabb, D.C. Liebler, and M.J. MacCoss. 2010. Skyline: An open source document editor for creating and analyzing targeted proteomics experiments. *Bioinformatics.* 26:966–968. http://dx.doi.org/10.1093/bioinformatics/btq054

Madisen, L., T.A. Zwingman, S.M. Sunkin, S.W. Oh, H.A. Zariwala, H. Gu, L.L. Ng, R.D. Palmiter, M.J. Hawrylycz, A.R. Jones, et al. 2010. A robust and high-throughput Cre reporting and characterization system for the whole mouse brain. *Nat. Neurosci.* 13:133–140. http://dx.doi.org/10.1038/nn.2467

Masuda, M., D. Dulon, K. Pak, L.M. Mullen, Y. Li, L. Erkman, and A.F. Ryan. 2011. Regulation of POU4F3 gene expression in hair cells by 5′ DNA in mice. *Neuroscience.* 197:48–64. http://dx.doi.org/10.1016/j.neuroscience.2011.09.033

Matei, V., S. Pauley, S. Kaing, D. Rowitch, K.W. Beisel, K. Morris, F. Feng, K. Jones, J. Lee, and B. Fritzsch. 2005. Smaller inner ear sensory epithelia in Neurog 1 null mice are related to earlier hair cell cycle exit. *Dev. Dyn.* 234:633–650. http://dx.doi.org/10.1002/dvdy.20551

Mburu, P., M.R. Romero, H. Hilton, A. Parker, S. Townsend, Y. Kikkawa, and S.D. Brown. 2010. Gelsolin plays a role in the actin polymerization complex of hair cell stereocilia. *PLoS One.* 5:e11627. http://dx.doi.org/10.1371/journal.pone.0011627

Mejillano, M.R., S. Kojima, D.A. Applewhite, F.B. Gertler, T.M. Svitkina, and G.G. Borisy. 2004. Lamellipodial versus filopodial mode of the actin nanomachinery: Pivotal role of the filament barbed end. *Cell.* 118:363–373. http://dx.doi.org/10.1016/j.cell.2004.07.019

Michelot, A., and D.G. Drubin. 2011. Building distinct actin filament networks in a common cytoplasm. *Curr. Biol.* 21:R560–R569. http://dx.doi.org/10.1016/j.cub.2011.06.019

Morgan, C.P., J.F. Krey, M. Grati, B. Zhao, S. Fallen, A. Kannan-Sundhari, X.Z. Liu, D. Choi, U. Müller, and P.G. Barr-Gillespie. 2016. PDZD7-MYO7A complex identified in enriched stereocilia membranes. *eLife.* 5:e18312. http://dx.doi.org/10.7554/eLife.18312

Moseley, J.B., K. Okada, H.I. Balcer, D.R. Kovar, T.D. Pollard, and B.L. Goode. 2006. Twinfilin is an actin-filament-severing protein and promotes rapid turnover of actin structures in vivo. *J. Cell Sci.* 119:1547–1557. http://dx.doi.org/10.1242/jcs.02860

Müller, C.B., and J. Enderlein. 2010. Image scanning microscopy. *Phys. Rev. Lett.* 104:198101. http://dx.doi.org/10.1103/PhysRevLett.104.198101

Narayanan, P., P. Chatterton, A. Ikeda, S. Ikeda, D.P. Corey, J.M. Ervasti, and B.J. Perrin. 2015. Length regulation of mechanosensitive stereocilia depends on very slow actin dynamics and filament-severing proteins. *Nat. Commun.* 6:6855. http://dx.doi.org/10.1038/ncomms7855

Odeh, H., K.L. Hunker, I.A. Belyantseva, H. Azaiez, M.R. Avenarius, L. Zheng, L.M. Peters, L.H. Gagnon, N. Hagiwara, M.J. Skynner, et al. 2010. Mutations in Grxcr1 are the basis for inner ear dysfunction in the pirouette mouse. *Am. J. Hum. Genet.* 86:148–160. http://dx.doi.org/10.1016/j.ajhg.2010.01.016

Olt, J., P. Mburu, S.L. Johnson, A. Parker, S. Kuhn, M. Bowl, W. Marcotti, and S.D. Brown. 2014. The actin-binding proteins eps8 and gelsolin have complementary roles in regulating the growth and stability of mechanosensory hair bundles of mammalian cochlear outer hair cells. *PLoS One.* 9:e87331. http://dx.doi.org/10.1371/journal.pone.0087331

Paavilainen, V.O., M. Hellman, E. Helfer, M. Bovellan, A. Annila, M.F. Carlier, P. Permi, and P. Lappalainen. 2007. Structural basis and evolutionary origin of actin filament capping by twinfilin. *Proc. Natl. Acad. Sci. USA.* 104:3113–3118. http://dx.doi.org/10.1073/pnas.0608725104

Palmgren, S., P.J. Ojala, M.A. Wear, J.A. Cooper, and P. Lappalainen. 2001. Interactions with PIP2, ADP-actin monomers, and capping protein regulate the activity and localization of yeast twinfilin. *J. Cell Biol.* 155:251–260. http://dx.doi.org/10.1083/jcb.200106157

Pan, N., I. Jahan, J. Kersigo, J.S. Duncan, B. Kopecky, and B. Fritzsch. 2012. A novel Atoh1 "self-terminating" mouse model reveals the necessity of proper Atoh1 level and duration for hair cell differentiation and viability. *PLoS One.* 7:e30358. http://dx.doi.org/10.1371/journal.pone.0030358

Patel, M.S., N.S. Nemeria, W. Furey, and F. Jordan. 2014. The pyruvate dehydrogenase complexes: Structure-based function and regulation. *J. Biol. Chem.* 289:16615–16623. http://dx.doi.org/10.1074/jbc.R114.563148

Peng, A.W., I.A. Belyantseva, P.D. Hsu, T.B. Friedman, and S. Heller. 2009. Twinfilin 2 regulates actin filament lengths in cochlear stereocilia. *J. Neurosci.* 29:15083–15088. http://dx.doi.org/10.1523/JNEUROSCI.2782-09.2009

Remmert, K., D. Vullhorst, and H. Hinssen. 2000. In vitro refolding of heterodimeric CapZ expressed in *E. coli* as inclusion body protein. *Protein Expr. Purif.* 18:11–19. http://dx.doi.org/10.1006/prep.1999.1132

Rodnick-Smith, M., Q. Luan, S.L. Liu, and B.J. Nolen. 2016. Role and structural mechanism of WASP-triggered conformational changes in branched actin filament nucleation by Arp2/3 complex. *Proc. Natl. Acad. Sci. USA.* 113:E3834–E3843. http://dx.doi.org/10.1073/pnas.1517798113

Roth, S., C.J. Sheppard, and R. Heintzmann. 2016. Superconcentration of light: Circumventing the classical limit to achievable irradiance. *Opt. Lett.* 41:2109–2112. http://dx.doi.org/10.1364/OL.41.002109

Rzadzinska, A.K., E.M. Nevalainen, H.M. Prosser, P. Lappalainen, and K.P. Steel. 2009. MyosinVIIa interacts with Twinfilin-2 at the tips of mechanosensory stereocilia in the inner ear. *PLoS One.* 4:e7097. http://dx.doi.org/10.1371/journal.pone.0007097

Schafer, D.A., P.B. Jennings, and J.A. Cooper. 1996. Dynamics of capping protein and actin assembly in vitro: Uncapping barbed ends by polyphosphoinositides. *J. Cell Biol.* 135:169–179. http://dx.doi.org/10.1083/jcb.135.1.169

Scheffer, D.I., J. Shen, D.P. Corey, and Z.Y. Chen. 2015. Gene expression by mouse inner ear hair cells during development. *J. Neurosci.* 35:6366–6380. http://dx.doi.org/10.1523/JNEUROSCI.5126-14.2015

Schwanhäusser, B., D. Busse, N. Li, G. Dittmar, J. Schuchhardt, J. Wolf, W. Chen, and M. Selbach. 2011. Global quantification of mammalian gene expression control. *Nature.* 473:337–342. http://dx.doi.org/10.1038/nature10098

Sekerková, G., C.P. Richter, and J.R. Bartles. 2011. Roles of the espin actin-bundling proteins in the morphogenesis and stabilization of hair cell stereocilia revealed in CBA/CaJ congenic jerker mice. *PLoS Genet.* 7:e1002032. http://dx.doi.org/10.1371/journal.pgen.1002032

Sheppard, C.J., S.B. Mehta, and R. Heintzmann. 2013. Superresolution by image scanning microscopy using pixel reassignment. *Opt. Lett.* 38:2889–2892. http://dx.doi.org/10.1364/OL.38.002889

Shin, J.B., J.F. Krey, A. Hassan, Z. Metlagel, A.N. Tauscher, J.M. Pagana, N.E. Sherman, E.D. Jeffery, K.J. Spinelli, H. Zhao, et al. 2013. Molecular architecture of the chick vestibular hair bundle. *Nat. Neurosci.* 16:365–374. http://dx.doi.org/10.1038/nn.3312

Sinnar, S.A., S. Antoku, J.M. Saffin, J.A. Cooper, and S. Halpain. 2014. Capping protein is essential for cell migration in vivo and for filopodial morphology and dynamics. *Mol. Biol. Cell.* 25:2152–2160. http://dx.doi.org/10.1091/mbc.E13-12-0749

Soeno, Y., H. Abe, S. Kimura, K. Maruyama, and T. Obinata. 1998. Generation of functional β-actinin (CapZ) in an *E. coli* expression system. *J. Muscle Res. Cell Motil.* 19:639–646. http://dx.doi.org/10.1023/A:1005329114263

Taylor, C.F., N.W. Paton, K.S. Lilley, P.A. Binz, R.K.J. Julian Jr., A.R. Jones, W. Zhu, R. Apweiler, R. Aebersold, E.W. Deutsch, et al. 2007. The minimum information about a proteomics experiment (MIAPE). *Nat. Biotechnol.* 25:887–893. http://dx.doi.org/10.1038/nbt1329

Tilney, L.G., and D.J. DeRosier. 1986. Actin filaments, stereocilia, and hair cells of the bird cochlea. IV. How the actin filaments become organized in developing stereocilia and in the cuticular plate. *Dev. Biol.* 116:119–129. http://dx.doi.org/10.1016/0012-1606(86)90048-5

Tilney, L.G., M.S. Tilney, and D.J. DeRosier. 1992. Actin filaments, stereocilia, and hair cells: How cells count and measure. *Annu. Rev. Cell Biol.* 8:257–274. http://dx.doi.org/10.1146/annurev.cb.08.110192.001353

Vartiainen, M.K., E.M. Sarkkinen, T. Matilainen, M. Salminen, and P. Lappalainen. 2003. Mammals have two twinfilin isoforms whose subcellular localizations and tissue distributions are differentially regulated. *J. Biol. Chem.* 278:34347–34355. http://dx.doi.org/10.1074/jbc.M303642200

Venable, J.D., M.Q. Dong, J. Wohlschlegel, A. Dillin, and J.R. Yates. 2004. Automated approach for quantitative analysis of complex peptide

mixtures from tandem mass spectra. *Nat. Methods.* 1:39–45. http://dx.doi.org/10.1038/nmeth705

Vizcaíno, J.A., E.W. Deutsch, R. Wang, A. Csordas, F. Reisinger, D. Ríos, J.A. Dianes, Z. Sun, T. Farrah, N. Bandeira, et al. 2014. ProteomeXchange provides globally coordinated proteomics data submission and dissemination. *Nat. Biotechnol.* 32:223–226. http://dx.doi.org/10.1038/nbt.2839

White, J.K., A.K. Gerdin, N.A. Karp, E. Ryder, M. Buljan, J.N. Bussell, J. Salisbury, S. Clare, N.J. Ingham, C. Podrini, et al. Sanger Institute Mouse Genetics Project. 2013. Genome-wide generation and systematic phenotyping of knockout mice reveals new roles for many genes. *Cell.* 154:452–464. http://dx.doi.org/10.1016/j.cell.2013.06.022

Wilmarth, P.A., J.F. Krey, J.B. Shin, D. Choi, L.L. David, and P.G. Barr-Gillespie. 2015. Hair-bundle proteomes of avian and mammalian inner-ear utricles. *Sci. Data.* 2:150074. http://dx.doi.org/10.1038/sdata.2015.74

Xiong, W., T. Wagner, L. Yan, N. Grillet, and U. Müller. 2014. Using injectoporation to deliver genes to mechanosensory hair cells. *Nat. Protoc.* 9:2438–2449. http://dx.doi.org/10.1038/nprot.2014.168

Zampini, V., L. Rüttiger, S.L. Johnson, C. Franz, D.N. Furness, J. Waldhaus, H. Xiong, C.M. Hackney, M.C. Holley, N. Offenhauser, et al. 2011. Eps8 regulates hair bundle length and functional maturation of mammalian auditory hair cells. *PLoS Biol.* 9:e1001048. http://dx.doi.org/10.1371/journal.pbio.1001048